

Scalar dark matter with Z_3 symmetry in Type-II Seesaw

AiGeng Yang and Hao Sun

Institute of Theoretical Physics, School of Physics, Dalian University of Technology, Dalian 116024, People's Republic of China

E-mail: aigengyang@mail.dlut.edu.cn, haosun@dlut.edu.cn

ABSTRACT: We study a simple complex scalar singlet dark matter (DM) model with Z_3 symmetry in the framework of type-II seesaw mechanism. We use the model to explain the excess of electron-positron flux measured by AMS-02, DAMPE and Fermi-LAT collaborations, which is encouraged by the decay of the triplets produced from dark matter annihilations in the Galactic halo. We focus on the non-degenerate case in which the mass of DM is larger than that of the triplets' and deliberately alleviate the leptophilic properties of the DM, so that the semi-annihilation effects are enhanced. With the guarantee of Z_3 symmetry, by fitting the antiproton spectrum observed in PAMELA and AMS experiments, we find that the DM cubic terms and the couplings between DM and Higgs are strongly constrained, leading to the semi-annihilation cross section fraction less than 3% when DM mass is given at 3 TeV.

KEYWORDS: Dark matter, Complex scalar singlet, Type-II Seesaw, Z_3 symmetry

Contents

1	Introduction	1
2	The model framework	3
2.1	The gauge part	3
2.2	The Yukawa part	4
2.3	The scalar potential	6
3	Constraints	9
3.1	Perturbativity	9
3.2	Perturbative unitarity	9
3.3	Vacuum stability	9
3.4	Globality of the Z_3 -symmetric vacuum	10
4	Phenomenology	13
4.1	Relic density and Direct restriction	13
4.2	Antiproton spectrum and electron-position flux	15
5	Summary	18
A	Appendix	19

1 Introduction

So far, there are at least two unsolved problems in particle physics: the nature of dark matter (DM) proved by astronomical evidence [1–6] and the origin of neutrino mass revealed by the observation of neutrino oscillations [7]. In terms of DM side, one of the research paradigm is the so-called weakly interacting massive particles (WIMPs) which can be regarded as DM candidates. Their masses are located in the weak scale and their interactions with the standard model (SM) particles are extremely tiny. Other paradigms of DM include Strongly Interacting Massive Particles (SIMPs) and Forbidden dark matter. The former is realized by (effective) five-point self-interactions [8–11], while the latter is the annihilation of hidden sector set opened at high temperature [8, 12, 13]. The Planck experiment [14] gives these paradigms constraint by its measured relic abundance: $\Omega h^2 = 0.1199 \pm 0.0027$ at the 2σ confidence level (C.L.). The direct detection experiments of, i.e., PandaX-II [15], also determined the DM properties, such as mass and couplings. For example, if DM particles are postulated to be extra singlet scalars beyond SM, especially in the so-called Higgs portal scenarios, they will only interact with SM Higgs doublet. On the other hand, in order to understand the origin of neutrino mass theoretically, several mechanisms have

been proposed, such as type I seesaw [16–18], by introducing heavy right-handed neutrinos, type II seesaw [19–26], by adding $SU(2)$ Higgs triplet, and so on [27–30].

In this paper, we try to combine the dark matter issue with neutrino mass issue and solve it in one framework. For the settlement of DM, we introduce a complex scalar singlet (S) with a global Z_3 symmetry, and treat it as a DM candidate. Its Z_3 charge is unity ($X_S = 1$) while the SM particles' are zero ($X_{SM} = 0$), the property of DM stability can therefore be guaranteed. This type of extended scalar could naturally be embedded in $SO(10)$ group on account of the same gauge and $B - L$ quantum number compared with SM fermions. Discrete symmetries such as Z_2 , Z_4 or Z_N have been presented in, for example, Refs.[31–36], in which the common feature can be selected that it is the remnant of breaking $U(1)_X$ gauge group [37, 38]. In addition, there have also been works on the complex scalar singlet under Z_3 symmetry. For example, Refs.[39, 40] study the SIMPs by introducing an extra nonzero vacuum expectation value (VEV) of dark Higgs field with Z_3 symmetry and provide DM candidates in the mass range of $\mathcal{O}(1 - 100)$ MeV. Ref.[41] obtains an improved mass bounds by the study on Z_3 singlet dark matter with refined unitarity bounds and treatment of early kinetic decoupling. It indicates that two DM mass ranges, $(56.8 \sim 58.4) \text{ GeV} \leq m_{DM} \leq 62.8 \text{ GeV}$ and $m_{DM} \geq 122 \text{ GeV}$, are permissive when the semi-annihilation processes play the role in freeze-out. Note when $N \geq 2$, the semi-annihilation arise if cubic terms exist among the dark matter or dark sector [36, 42]. On the other hand, in order to explain the origin of neutrino masses, we introduce a $SU(2)$ scalar triplet Δ with Z_3 charge $X_\Delta = 0$. This triplet state will obtain a small nonzero VEV after electroweak symmetry breaking (EWSB), and leads to the Majorana mass origin of neutrinos through Yukawa couplings of leptons and triplets. A further reason to introduce the triplet is its role in exploring the observed excess of cosmic-ray observed in the electron-positron flux measured by the AMS-02 [43], Fermi-LAT [44] and DAMPE [45] experiments, due to the leptonic decays of such triplet in DM annihilation [46–48]. In addition, the other method based on a Z_3 stabilized DM and a two-loop induced neutrino mass, has also been used to explain the electron-positron spectrum, see in Ref.[49–51]. In short, in this paper we extend the SM with a complex singlet scalar and a scalar triplet undergoing $SU(2)_L \otimes U(1)_Y \otimes Z_3$ symmetry as our model framework.

In our paper we focus on the study of heavy DM case, say, annihilation of DM particles with masses larger than $\mathcal{O}(1)$ TeV. The boost factor (BF) is also necessary to be considered which may come from large inhomogeneities in the dark matter distribution or due to the so-called Breit Wigner enhancement mechanism in particle physics [52–54]. Note that the leptophilic dark matter (LDP) mechanism, in which a pair of DM particles mainly annihilates into a pair of triplet, is often adopted to fit the excess of electron-positron spectrum [46, 47]. There, the coupling between DM and Higgs is naturally negligible, leading to negligible semi-annihilation effects. In our model, the semi-annihilation effects may contribute due to the remarkable characteristics of Z_3 symmetry. We therefore deliberately alleviate the LDP mechanism and reinforce the semi-annihilation effects to see how they would be constrained accordingly. As can be seen, the W and Z boson pair from s-channel DM annihilation with subsequent decay may lead to inappropriate antiproton spectrum measured by AMS[55] and PAMELA[56] in cosmic-ray, therefore set limits to the BF and the λ_{SH}

coupling between DM and Higgs, and the corresponding desirable semi-annihilation cross section fraction is obtained.

The paper is organized as follows. In Sec.2, we set up the model framework including the gauge, the Yukawa and the scalar sectors. In Sec.3, we derive the theoretical constraints, especially the globality of the Z_3 symmetry vacuum is studied. In Sec.4, we provide the detailed phenomenological studies and present our numerical results. Finally, a short summary is given in Sec.5.

2 The model framework

We extend the SM by introducing a scalar singlet S (stabilised by a Z_3 symmetry), which can be considered as the dark matter candidate. The scalar triplet Δ of hypercharge $Y=2$ is also added to this model in order to generate the masses of neutrinos. Considering that the new Z_3 symmetry keeps the scalar potential invariant, the corresponding transformations are: $H \rightarrow H$, $\Delta \rightarrow \Delta$, $S \rightarrow e^{i2\pi/3}S$. We choose Z_3 charge of S equal $X_S=1$, and the others with Z_3 charges zero. The field S will not develop a VEV after EWSB due to the existence of Z_3 symmetry, and will play the role of dark matter candidate.

The total Lagrangian of the model can be written as

$$\mathcal{L}_{\text{tot}} = \mathcal{L}_{\text{Kinetic}} + \mathcal{L}_{\text{Yukawa}} - \mathcal{V}(H, \Delta, S), \quad (2.1)$$

with the kinetic and Yukawa terms are

$$\mathcal{L}_{\text{Kinetic}} = (D^\mu H)^\dagger D_\mu H + (D^\mu \Delta)^\dagger D_\mu \Delta + (\partial^\mu S)^\dagger \partial_\mu S, \quad (2.2)$$

$$\mathcal{L}_{\text{Yukawa}} = \mathcal{L}_{\text{Yukawa}}^{\text{SM}} - \frac{Y_{ij}}{2} L_i^T \mathcal{C} i \sigma_2 \Delta L_j + \text{h.c.} . \quad (2.3)$$

Here Y_{ij} represents the Yukawa coupling, $L_{i,j}$ are the $SU(2)_L$ doublet of left hand leptons, i, j are the generation index and \mathcal{C} is the charge conjugation operator. Obviously there are no couplings involved between the scalar singlet S and the SM fermions. The scalar potential \mathcal{V} will be discussed in detail later. H and Δ are labels of the Higgs doublet and scalar triplet respectively which are represented as

$$H = \begin{pmatrix} G^+ \\ \frac{1}{\sqrt{2}}(v_0 + h + iG^0) \end{pmatrix}, \quad (2.4)$$

$$\Delta = \begin{pmatrix} \frac{1}{\sqrt{2}}\delta^+ & \delta^{++} \\ \frac{1}{\sqrt{2}}(v_\Delta + \delta^0 + i\eta^0) & -\frac{1}{\sqrt{2}}\delta^+ \end{pmatrix} \text{ or } \begin{pmatrix} \delta^{++} \\ \delta^+ \\ \frac{1}{\sqrt{2}}(v_\Delta + \delta^0 + i\eta^0) \end{pmatrix} \quad (2.5)$$

with v_0 (v_Δ) is the VEV of H (Δ). And for S we have $v_S = 0$. G^0 , G^\pm are the Goldstone bosons which are eaten up to give mass to SM gauge bosons.

2.1 The gauge part

In Eq.(2.2), the covariant derivatives can be expressed as

$$D_\mu = \partial_\mu + i\frac{g}{\sqrt{2}}(T^+ W_\mu^+ + T^- W_\mu^-) + i\frac{g}{c_W}(T^3 - s_W^2 Q)Z_\mu + ieQA_\mu \quad (2.6)$$

where W_μ^\pm , Z_μ and A_μ are the SM gauge bosons, g is the gauge coupling of $SU(2)_L$ and θ_W stands for Weinberg angle with $s_W(c_W) = \sin\theta_W(\cos\theta_W)$ for short. Q is the charge operator. For scalar doublet, T are associated to Pauli matrices by

$$T^\pm = \frac{1}{2}(\sigma_1 \pm \sigma_2), \quad T^3 = \sigma_3 \quad (2.7)$$

and $Q = \text{diag}(1, 0)$. While for the scalar triplet we have $Q = \text{diag}(2, 1, 0)$ and $T^\pm = T^1 \pm iT^2$ with the $SU(2)_L$ generators chosen as

$$T^1 = \frac{1}{\sqrt{2}} \begin{pmatrix} 0 & 1 & 0 \\ 1 & 0 & 1 \\ 0 & 1 & 0 \end{pmatrix}, T^2 = \frac{1}{\sqrt{2}} \begin{pmatrix} 0 & -i & 0 \\ i & 0 & -i \\ 0 & i & 0 \end{pmatrix}, T^3 = \begin{pmatrix} 1 & 0 & 0 \\ 0 & 0 & 0 \\ 0 & 0 & -1 \end{pmatrix}. \quad (2.8)$$

The kinetic terms of triplet Δ will change the SM W^\pm and Z gauge boson masses, which can be expressed after spontaneous symmetry breaking as

$$m_W^2 = \frac{g^2 v_0^2}{4} \left(1 + \frac{2v_\Delta^2}{v_0^2}\right), \quad m_Z^2 = \frac{g^2 v_0^2}{4c_W^2} \left(1 + \frac{4v_\Delta^2}{v_0^2}\right), \quad (2.9)$$

therefore affect the SM ρ parameter at tree level

$$\rho = \frac{m_W^2}{m_Z^2 c_W^2} = \frac{1 + 2v_\Delta^2/v_0^2}{1 + 4v_\Delta^2/v_0^2}. \quad (2.10)$$

The current electroweak precision data constraints require the ρ parameter to $1.0004_{-0.0004}^{+0.0003}$ [57] and thus give

$$\frac{v_\Delta}{v_0} \lesssim 0.02, \quad \text{or} \quad v_\Delta \lesssim 5 \text{ GeV}, \quad (2.11)$$

suppose the VEV of Higgs doublet satisfy $\sqrt{v_0^2 + 2v_\Delta^2} = 246.22 \text{ GeV}$. Hence we are safe in the region $v_\Delta \ll v_0$. We can easily find out that the gauge interactions of triplet particles such as $\delta^0 W^+ W^-$ and $\delta^0 Z Z$ vertexes, are all proportional to v_Δ . More detailed discussion can be found in Ref.[58]. Since in our case we consider the singlet scalar, there is no direct connection between S and gauge fields.

2.2 The Yukawa part

The triplet scalars coupling with the leptons through Type-II Seesaw mechanism are given, in terms of Yukawa matrix \mathbf{Y} , by

$$\mathcal{L}_{\text{Yukawa}}^{\text{New}} = -\frac{1}{2} L^T \mathcal{C} \mathbf{Y} i \sigma_2 \Delta L + \text{h.c.}, \quad (2.12)$$

with $\mathcal{C} = i\gamma_0\gamma_2$. $L^T = (\nu_\ell^T, \ell^T)$ is the transpose of the $SU(2)_L$ left handed lepton doublet mentioned above. We can simply obtain the expanded expression

$$\mathcal{L}_{\text{Yukawa}}^{\text{New}} = -\frac{Y_{ij}}{2} \nu_i^T \mathcal{C} \nu_j \frac{v_\Delta + \delta^0 + i\eta^0}{\sqrt{2}} + Y_{ij} \nu_i^T \mathcal{C} \ell_j \frac{\delta^+}{\sqrt{2}} + \frac{Y_{ij}}{2} \ell_i^T \mathcal{C} \ell_j \delta^{++} + \text{h.c.}, \quad (2.13)$$

with $i, j = 1, 2, 3$. Therefore \mathbf{Y} is related to the Majorana neutrino mass matrix in flavour eigenstates by $\mathbf{m}_\nu = v_\Delta \mathbf{Y} / \sqrt{2}$. Assume the physical neutrino mass matrix is $\mathbf{m}_\nu^{\text{diag}} = \text{diag}(m_1, m_2, m_3)$, with the help of Pontecorvo-Maki-Nakagawa-Sakata (PMNS) matrix U_{PMNS} , the Yukawa matrix can thus be written as

$$\mathbf{Y} = \frac{\sqrt{2}}{v_\Delta} U_{PMNS}^* \mathbf{m}_\nu^{\text{diag}} U_{PMNS}^\dagger = \frac{\sqrt{2}}{v_\Delta} \begin{pmatrix} m_{ee} & m_{e\mu} & m_{e\tau} \\ m_{e\mu} & m_{\mu\mu} & m_{\mu\tau} \\ m_{e\tau} & m_{\mu\tau} & m_{\tau\tau} \end{pmatrix}. \quad (2.14)$$

The U_{PMNS} matrix can be parametrized by

$$U_{PMNS} = \begin{pmatrix} c_{12}c_{13} & c_{13}s_{12} & e^{-i\delta}s_{13} \\ -c_{12}s_{13}s_{23}e^{i\delta} - c_{23}s_{12} & c_{12}c_{23} - e^{i\delta}s_{12}s_{13}s_{23} & c_{13}s_{23} \\ s_{12}s_{23} - e^{i\delta}c_{12}c_{23}s_{13} & -c_{23}s_{12}s_{13}e^{i\delta} - c_{12}s_{23} & c_{13}c_{23} \end{pmatrix} \\ \times \text{diag} \left(e^{i\Phi_1/2}, 1, e^{i\Phi_2/2} \right) \quad (2.15)$$

with $s_{ij} = \sin \theta_{ij}$, $c_{ij} = \cos \theta_{ij}$ and δ, Φ_i are the Dirac, Majorana CP phases respectively. For illustration purpose, we set the two Majorana phases and the lightest neutrino mass to be zero and the masses obey

- The normal hierarchy (NH) scenario ($m_1 < m_2 < m_3$) with $m_2 = (m_1^2 + \Delta m_{21}^2)^{1/2}$, $m_3 = (m_1^2 + \Delta m_{31}^2)^{1/2}$,
- The inverted hierarchy (IH) scenario ($m_3 < m_1 < m_2$) with $m_1 = (m_3^2 + \Delta m_{31}^2)^{1/2}$, $m_2 = (m_1^2 + \Delta m_{21}^2)^{1/2}$,

where $\Delta m_{ij}^2 = m_i^2 - m_j^2$. Using the central values of the global analysis based on the neutrino oscillation data [59]:

$$\Delta m_{21}^2 = 7.50 \times 10^{-5} \text{eV}^2, \quad |\Delta m_{31}^2| = 2.524(2.514) \times 10^{-3} \text{eV}^2, \\ \sin^2 \theta_{12} = 0.306, \quad \sin^2 \theta_{23} = 0.441(0.587), \\ \delta = 261^\circ (277^\circ), \quad \sin^2 \theta_{13} = 0.02166 (0.02179), \quad (2.16)$$

where the values in parentheses correspond to the IH scenario, we obtain the Yukawa coupling matrix

$$\mathbf{Y}^{\text{NH}} = \frac{10^{-2} \text{eV}}{v_\Delta} \times \begin{pmatrix} 0.1558 + 0.0336i & 0.2232 - 0.5050i & -0.3432 - 0.5686i \\ 0.2232 - 0.5050i & 2.5103 - 0.0584i & 1.0963 - 0.03901i \\ 2.1403 - 0.0078i & 1.0963 - 0.0390i & 3.0004 + 0.0566i \end{pmatrix}, \quad (2.17)$$

and

$$\mathbf{Y}^{\text{IH}} = \frac{10^{-2} \text{eV}}{v_\Delta} \times \begin{pmatrix} 3.6631 & -1.2660 - 0.4156i & 1.4057 - 0.3487i \\ -1.2660 - 0.4158i & 0.8693 + 0.2874i & -1.0963 - 0.03901i \\ 1.4057 - 0.3487i & -1.0963 - 0.03901i & 1.1869 - 0.2676i \end{pmatrix}. \quad (2.18)$$

With the help of these known Yukawa coupling values, the branching ratios of the triplet scalars can be calculated and listed in Table 1 for both the IH and NH scenarios. The decay of $\delta^{\pm\pm}$ final states produces a fraction of $e : \mu : \tau \approx 1 : 0.2 : 0.3$ and $1 : 0.5 : 1.4$ in IH and NH scenario, respectively. The electron-rich final states in IH case is pointing to the excess of the spectrum indicated by the AMS-02, DAMPE and Fermi-LAT measurements. We will give more detailed discussion in the following section.

$\delta^{\pm\pm}$	IH	NH	δ^0/η^0	IH	NH	δ^\pm	IH	NH
$\text{Br}(e^\pm e^\pm)$	51.80%	1.32%	$\text{Br}(\nu_e \nu_e)$	51.80%	1.32%	$\text{Br}(e^\pm \nu_e)$	51.80%	1.32%
$\text{Br}(\mu^\pm \mu^\pm)$	3.24%	3.28%	$\text{Br}(\nu_\mu \nu_\mu)$	3.24%	3.28%	$\text{Br}(e^\pm \nu_\mu)$	6.86%	1.58%
$\text{Br}(\tau^\pm \tau^\pm)$	5.72%	4.68%	$\text{Br}(\nu_\tau \nu_\tau)$	5.72%	4.68%	$\text{Br}(e^\pm \nu_\tau)$	8.10%	22.9%
$\text{Br}(e^\pm \mu^\pm)$	13.70%	31.7%	$\text{Br}(\nu_e \nu_\mu)$	13.70%	31.7%	$\text{Br}(\mu^\pm \nu_e)$	6.86%	1.58%
$\text{Br}(e^\pm \tau^\pm)$	16.20%	45.9%	$\text{Br}(\nu_e \nu_\tau)$	16.20%	45.9%	$\text{Br}(\mu^\pm \nu_\mu)$	3.24%	3.28%
$\text{Br}(\mu^\pm \tau^\pm)$	9.30%	1.25%	$\text{Br}(\nu_\mu \nu_\tau)$	9.30%	1.25%	$\text{Br}(\mu^\pm \nu_\tau)$	4.65%	6.26%
						$\text{Br}(\tau^\pm \nu_e)$	8.10%	22.9%
						$\text{Br}(\tau^\pm \nu_\mu)$	4.65%	62.6%
						$\text{Br}(\tau^\pm \nu_\tau)$	5.72%	4.68%

Table 1: Branching ratios (Br) of triplet scalars decay calculated by CalcHEP [60] in NH, IH scenarios, with the corresponding Yukawa coupling values listed in Eq.(2.17) and Eq.(2.18).

The singly- and doubly-charged scalars in the type-II Seesaw model also contribute to the lepton flavor violating (LFV) processes, therefore put astringent lower bounds based on the current experiment [61, 62], given $v_\Delta M_\Delta \cdot \geq 150 \text{ eV} \cdot \text{GeV}$, where M_Δ is the triplet mass. The limits from LHC direct searches for doubly charged Higgs bosons also require $M_\Delta \gtrsim 770 - 870 \text{ GeV}$ [63, 64]. We will take $v_\Delta = 1 \text{ eV}$ in our following analysis.

2.3 The scalar potential

The general scalar potential in our case is given by

$$\begin{aligned}
\mathcal{V}(H, \Delta, S) = & m_h^2 H^\dagger H + \lambda |H|^4 + M_\Delta^2 \text{Tr}(\Delta^\dagger \Delta) + \mu_S^2 S^\dagger S + \lambda_S (S^\dagger S)^2 \\
& + [\mu_1 (H^T i\sigma^2 \Delta^\dagger H) + \text{h.c.}] + \lambda_1 (H^\dagger H) \text{Tr}(\Delta^\dagger \Delta) + \lambda_2 (\text{Tr} \Delta^\dagger \Delta)^2 \\
& + \lambda_3 \text{Tr}(\Delta^\dagger \Delta)^2 + \lambda_4 H^\dagger \Delta \Delta^\dagger H + \lambda_{SH} |S|^2 |H|^2 \\
& + \lambda_{S\Delta} |S|^2 \text{Tr}(\Delta^\dagger \Delta) + \frac{\mu_3}{2} (S^3 + S^{\dagger 3}). \tag{2.19}
\end{aligned}$$

The full scalar part can be split into two parts:

$$\mathcal{V}(H, \Delta, S) = \mathcal{V}_{\text{nonDM}} + \mathcal{V}_{\text{DM}} \tag{2.20}$$

with

$$\mathcal{V}_{\text{DM}} = \mu_S^2 S^\dagger S + \lambda_S (S^\dagger S)^2 + \lambda_{SH} |S|^2 |H|^2 + \lambda_{S\Delta} |S|^2 \text{Tr}(\Delta^\dagger \Delta) + \frac{\mu_3}{2} (S^3 + S^{\dagger 3}), \tag{2.21}$$

where the cubic item $(S^3 + S^{\dagger 3})$ keeps Z_3 symmetry invariance through $(S^3 + S^{\dagger 3}) \rightarrow ((e^{i2\pi/3}S)^3 + (e^{-i2\pi/3}S^\dagger)^3)$ transformation, the parameter μ_3 can be regarded as real, owing to its phase can be absorbed into the phase of the singlet S , and not necessary to be negative due to $\frac{\mu_3}{2}(S^3 + S^{\dagger 3}) \rightarrow -\frac{\mu_3}{2}((-S)^3 + (-S)^\dagger{}^3)$ changing invariance. The other parameters are also regarded as real for ignoring the CP related issues. When the EWSB is triggered by the condition of $\mu^2 < 0$, the SM doublet H obtain a VEV $v_0 \approx 246.22$ GeV and we fix the Higgs mass to be $m_h = 125$ GeV.

In the following, we summarize the key formulas we use in our model implementation, while recommend Ref.[65] for a more detailed description. When the doublet H and the triplet Δ get the VEVs, we obtain

$$\mathcal{V}(v_0, v_\Delta, 0) = \frac{m_h^2}{2}v_0^2 + \frac{\lambda}{4}v_0^4 + \frac{M_\Delta^2}{2}v_\Delta^2 + \frac{\lambda_1 + \lambda_4}{4}v_0^2v_\Delta^2 + \frac{\lambda_2 + \lambda_3}{4}v_\Delta^4 - \frac{\mu_1}{\sqrt{2}}v_0^2v_\Delta. \quad (2.22)$$

By solving the minimal condition of $\partial\mathcal{V}(v_0, v_\Delta, 0)/\partial v_\Delta = 0$ and $\partial\mathcal{V}(v_0, v_\Delta, 0)/\partial v_0 = 0$ under the condition $v_\Delta \ll v_0$, we can get

$$v_0 = \sqrt{\frac{-\mu^2}{\lambda}}, \quad v_\Delta \approx \frac{\mu_1 v_0^2}{\sqrt{2}(M_\Delta^2 + \frac{\lambda_1 + \lambda_4}{2}v_0^2)}. \quad (2.23)$$

The value of μ_1 is small in the scheme of $\mu_1 \sim v_\Delta$ so that we can neglect the associated effects in DM annihilation. The doubly charged mass eigenvalue could also be obtained by collecting the coefficients of $\delta^{\pm\pm}$ in the potential. It reads

$$M_{\delta^{\pm\pm}}^2 = -v_\Delta^2\lambda_3 - \frac{\lambda_4}{2}v_0^2 + \frac{\mu_1}{\sqrt{2}}\frac{v_0^2}{v_\Delta}. \quad (2.24)$$

Here and in the following, without confusion, we use the flavor eigenstate symbol to label its mass eigenstate. The mass squared matrix for the singly charged field can be diagonalized, with one eigenvalue zero corresponding to the charged Goldstone boson G^\pm while the other corresponds to the singly charged Higgs boson δ^\pm and is given by

$$M_{\delta^\pm}^2 = -\frac{v_0^2 + 2v_\Delta^2}{4v_\Delta}(v_\Delta\lambda_4 - 2\sqrt{2}\mu_1). \quad (2.25)$$

When the neutral scalar mass matrix is diagonalized, one obtains two massive even-parity physical states h and δ^0 with the masses given by the eigenvalues

$$M_h^2 = \frac{1}{2}(A + B - \sqrt{(A - B)^2 + 4C^2}), \quad (2.26)$$

$$M_{\delta^0}^2 = \frac{1}{2}(A + B + \sqrt{(A - B)^2 + 4C^2}). \quad (2.27)$$

with

$$A = 2v_0^2\lambda, \quad (2.28)$$

$$B = 2v_\Delta^2(\lambda_2 + \lambda_3) + \frac{\mu_1}{\sqrt{2}}\frac{v_0^2}{v_\Delta}, \quad (2.29)$$

$$C = v_0(v_\Delta(\lambda_1 + \lambda_4) - \sqrt{2}\mu_1). \quad (2.30)$$

The pseudoscalar mass matrices leads to one massless Goldstone boson G^0 and one massive physical state η^0

$$M_{\eta^0}^2 = \frac{v_0^2 + 4v_\Delta^2}{\sqrt{2}v_\Delta} \mu_1. \quad (2.31)$$

From the relation listed above we can write the coupling parameters as function of the masses

$$\mu_1 = \frac{\sqrt{2}v_\Delta}{v_0^2 + 4v_\Delta^2} M_{\eta^0}^2, \quad (2.32)$$

$$\lambda = \frac{1}{2v_0^2} (M_h^2 \cos^2 \beta + M_{\delta^0}^2 \sin^2 \beta), \quad (2.33)$$

$$\lambda_4 = \frac{4}{v_0^2 + 4v_\Delta^2} M_{\eta^0}^2 - \frac{4}{v_0^2 + 2v_\Delta^2} M_{\delta^\pm}^2, \quad (2.34)$$

$$\lambda_3 = \frac{1}{v_\Delta^2} \left(\frac{-v_0^2}{v_0^2 + 4v_\Delta^2} M_{\eta^0}^2 + \frac{2v_0^2}{v_0^2 + 2v_\Delta^2} M_{\delta^\pm}^2 - m_{\delta^{\pm\pm}}^2 \right), \quad (2.35)$$

$$\lambda_2 = \frac{1}{v_\Delta^2} \left(\frac{\sin^2 \beta M_h^2 + \cos^2 \beta M_{\delta^0}^2}{2} + \frac{1}{2} \frac{v_0^2}{v_0^2 + 4v_\Delta^2} M_{\eta^0}^2 - \frac{2v_0^2}{v_0^2 + 2v_\Delta^2} M_{\delta^\pm}^2 + M_{\delta^{\pm\pm}}^2 \right), \quad (2.36)$$

$$\lambda_1 = -\frac{2}{v_0^2 + 4v_\Delta^2} M_{\eta^0}^2 + \frac{4}{v_0^2 + 2v_\Delta^2} M_{\delta^\pm}^2 + \frac{\sin 2\beta}{2v_0 v_\Delta} (M_h^2 - M_{\delta^0}^2). \quad (2.37)$$

with the mixing angle β satisfies

$$\sin(2\beta) = \frac{4v_0 [-5(4M_\Delta^2 + 2(M_h^2 + M_{\delta^0}^2) + M_h^2) v_\Delta^2 (v_0^2 + 4v_\Delta^2) + M_\eta^2 (4v_0^4 + 6v_0^2 v_\Delta^2 + 5v_\Delta^4)]}{5(M_h^2 - M_{\delta^0}^2) v_\Delta (4v_0^2 + v_\Delta^2) (v_0^2 + 4v_\Delta^2)}. \quad (2.38)$$

Finally for the dark matter part, we obtain

$$M_S^2 = \mu_S^2 + \frac{\lambda_{SH}}{2} v_0^2 + \frac{\lambda_{S\Delta}}{2} v_\Delta^2. \quad (2.39)$$

Some other basic relations that may useful are also list here: $g = e/s_W$, $e = \sqrt{4\pi\alpha_{ew}}$, $s_W^2 = \pi\alpha_{ew}/\sqrt{2}/G_f/M_W^2$, $v_0^2 = \sqrt{1/\sqrt{2}G_f - 2v_\Delta^2}$, $M_W = \sqrt{M_Z^2/2 + \sqrt{M_Z^4/4 - M_Z^2\pi\alpha/\sqrt{2}/G_f}}$. We therefore choose our inputs as

$$\alpha_{ew}, M_Z, G_f, M_h \quad (2.40)$$

for the SM part and

$$v_\Delta, M_{\delta^{\pm\pm}}, M_{\delta^\pm}, M_{\delta^0}, M_{\eta^0} \quad (2.41)$$

for the triplet part and

$$M_S, \lambda_{SH}, \lambda_{S\Delta}, \mu_3 \quad (2.42)$$

for the dark matter part, respectively.

3 Constraints

3.1 Perturbativity

To illustrate the theoretical bounds from perturbativity behaviour of the dimensionless scalar quartic couplings, we follow the definitions in Refs.[35, 66]. As to the case of unrotated basis, the vertices from the potential must be less than 4π to make sure that the tree level contributions are larger than the one-loop level quantum corrections. This condition will give the constrains on the couplings λ_i in the potential, which are list here:

$$\begin{aligned}
 |6\lambda| &\leq 4\pi, |\lambda_1 + \lambda_4| \leq 4\pi, |\lambda_1| \leq 4\pi, \left|\lambda_1 + \frac{\lambda_4}{2}\right| \leq 4\pi, |6(\lambda_2 + \lambda_3)| \leq 4\pi, \\
 |2\lambda_2| &\leq 4\pi, |2(2\lambda_2 + \lambda_3)| \leq 4\pi, |\sqrt{2}\lambda_3| \leq 4\pi, |\lambda_4| \leq 4\pi, \\
 |\lambda_{S\Delta}| &\leq 4\pi, |\lambda_{SH}| \leq 4\pi, |4\lambda_S| \leq 4\pi.
 \end{aligned}
 \tag{3.1}$$

3.2 Perturbative unitarity

The tree-level unitarity from two-body scalar-scalar scattering processes gives another bound on the couplings λ_i in the potential. When the collision energy \sqrt{s} becomes larger, the processes will be dominated by the terms of quartic contact interaction. Although the trilinear couplings contributed to scattering should be included at finite collision energy [41, 67], for simplicity, we only calculate unitarity constrains with the scenarios: $s \rightarrow +\infty$. Then the s-wave scattering amplitudes lay in the perturbative unitarity limit, give the constrain of the scalar-scalar scattering S-matrix values: $|\text{Re}\mathcal{M}_i| \leq \frac{1}{2}$. The perturbative unitarity in the type-II seesaw model has been studied with decomposing the matrix S by the mutually unmixed sets of channels with definite charge and CP states[65]. We extend the way of decomposing by considering the Z_3 symmetry and $X_S=1$ singlet S introduced in our model. The matrix S can be decomposed into seven submatrice blocks structured in terms of electric charges and Z_3 charges in the initial/final states. In Appendix A, we display the initial/final states E_i and the corresponding scattering submatrix \mathcal{M}_i . The corresponding eigenvalues e_i^j of each submatrix are then calculated. The limit from pertubative unitarity on the potential's couplings λ_i , i.e., $|\text{Re}\mathcal{M}_i| \leq \frac{1}{2}$, infers $|e_i| \leq 8\pi$.

3.3 Vacuum stability

When the scalar field becomes larger in any direction of the field space, the constraint from vacuum stability is necessary since the scalar potential energy has a finite minimum. In other words, the scalar potential must have a lower bound. The quadratic and cubic terms in the scalar potential can be ignored compared with quartic term in this limit. These constrains can be achieved by writing the matrix of quartic interaction on the basis of non-negative field variables and ensuring that the matrix \mathcal{M} to be copositive [35, 68].

To parametrize the fields, we can define [35, 65]:

$$\begin{cases} H^\dagger H = r_1^2, \\ S = se^{i\phi}, \\ Tr(\Delta^\dagger \Delta) = r_2^2, \\ Tr(\Delta^\dagger \Delta)^2 / (Tr \Delta^\dagger \Delta)^2 \equiv n_1, \quad n_1 \in [\frac{1}{2}, 1], \\ (H^\dagger \Delta \Delta^\dagger H) / (H^\dagger H Tr \Delta^\dagger \Delta) \equiv n_2, \quad n_2 \in [0, 1]. \end{cases} \quad (3.2)$$

The scalar potential about vacuum stability can be written:

$$\begin{aligned} \mathcal{V}(H, \Delta, S)_{\text{quartic}} &= \lambda |H|^4 + \lambda_S (S^\dagger S)^2 + \lambda_1 (H^\dagger H) Tr(\Delta^\dagger \Delta) + \lambda_2 (Tr \Delta^\dagger \Delta)^2 + \\ &\quad \lambda_3 Tr(\Delta^\dagger \Delta)^2 + \lambda_4 H^\dagger \Delta \Delta^\dagger H + \lambda_{SH} |S|^2 |H|^2 + \lambda_{S\Delta} |S|^2 Tr(\Delta^\dagger \Delta) \\ &= (r_1^2, r_2^2, s^2) \mathcal{M} \begin{pmatrix} r_1^2 \\ r_2^2 \\ s^2 \end{pmatrix}, \end{aligned} \quad (3.3)$$

where

$$\mathcal{M} = \begin{pmatrix} \lambda & \frac{\lambda_1 + n_2 \lambda_4}{2} & \frac{\lambda_{SH}}{2} \\ \frac{\lambda_1 + n_2 \lambda_4}{2} & \lambda_2 + \lambda_3 n_1 & \frac{\lambda_{S\Delta}}{2} \\ \frac{\lambda_{SH}}{2} & \frac{\lambda_{S\Delta}}{2} & \lambda_S \end{pmatrix} \quad (3.4)$$

is a 3×3 symmetric matrix. In Refs.[69, 70], the necessary and sufficient conditions for the matrix \mathcal{M} to be copositive had been considered. Then, the vacuum stability conditions are given below:

$$\begin{aligned} \lambda \geq 0, \quad \lambda_2 + \lambda_3 n_1 \geq 0, \quad \lambda_S \geq 0, \quad \frac{\lambda_1 + n_2 \lambda_4}{2} + \sqrt{\lambda(\lambda_2 + \lambda_3 n_1)} \geq 0, \\ \frac{\lambda_{SH}}{2} + \sqrt{\lambda \lambda_S} \geq 0, \quad \frac{\lambda_{S\Delta}}{2} + \sqrt{(\lambda_2 + \lambda_3 n_1) \lambda_S} \geq 0, \\ \sqrt{\lambda(\lambda_2 + \lambda_3 n_1) \lambda_S} + \frac{\lambda_1 + n_2 \lambda_4}{2} \sqrt{\lambda_S} + \frac{\lambda_{SH}}{2} \sqrt{\lambda_2 + \lambda_3 n_1} + \frac{\lambda_{S\Delta}}{2} \sqrt{\lambda} + \\ \sqrt{2 \left(\frac{\lambda_1 + n_2 \lambda_4}{2} + \sqrt{\lambda(\lambda_2 + \lambda_3 n_1)} \right) \left(\frac{\lambda_{SH}}{2} + \sqrt{\lambda \lambda_S} \right) \left(\frac{\lambda_{S\Delta}}{2} + \sqrt{(\lambda_2 + \lambda_3 n_1) \lambda_S} \right)} \geq 0. \end{aligned} \quad (3.5)$$

Here, $n_1 \in [\frac{1}{2}, 1]$ and $n_2 \in [0, 1]$.

3.4 Globality of the Z_3 -symmetric vacuum

Since we choose the complex singlet scalar S as the DM candidate, the Z_3 symmetry should remain unbroken. The vacuum stability condition leads to the existence of a finite global minimum in the scalar potential. To ensure that the SM (\overline{EW}, Z_3) vacuum is selected as the global minimum vacuum, we study the stationary points at the extrema of scalar potential. Follow the parametrizing of the fields in Eq.(3.2), the stationary points can be

obtained by taking the derivative of the potential $\mathcal{V}(r_1, r_2, s, \phi)$ with respect to r_1 , r_2 , s and ϕ respectively and solving the equations of

$$\begin{aligned}
0 &= r_1(2\lambda r_1^2 + \lambda_1 r_2^2 + \lambda_4 n_2 r_2^2 + \lambda_{SH} s^2 + m_h^2), \\
0 &= r_2(\lambda_1 r_1^2 + 2\lambda_2 r_2^2 + 2\lambda_3 n_1 r_2^2 + M_\Delta^2 + \lambda_4 n_2 r_1^2 + \lambda_{S\Delta} s^2), \\
0 &= s(4\lambda_S s^2 + 2\mu_S^2 + 2\lambda_{SH} r_1^2 + 2\lambda_{S\Delta} r_2^2 + 3\mu_3 s \cos(3\phi)), \\
0 &= s^3 \mu_3 \sin(3\phi).
\end{aligned} \tag{3.6}$$

Here, we have ignored μ_1 ($\mu_1 \sim \mu_\Delta$). We use Eq.(2.23-2.39) to simplify the form of solution of Eq.(3.6). The chosen scheme of triplet scalar mass degeneracy leads to $\lambda_3 \simeq 0$ and $\lambda_4 \simeq 0$. And since $v_\Delta \ll v_0$ so that $\lambda_1 \approx \lambda_2 \approx \frac{2M_h^2}{v_0^2}$. Due to the chosen condition of $\lambda_{S\Delta} > 0$, and $M_\Delta^2 > 0$, so we have $r_2 = 0$. We also set $\mu_3 \geq 0$ and $\cos 3\phi = -1$ to obtain a local minima of potential with $s \neq 0$ [42]. Finally, there are only four vacuums left that should be considered, we give the discussion below:

1. ($r_1 = 0, s = 0$) vacuum: electroweak (EW) and Z_3 symmetries keep unbroken, $v_h = v_\Delta = v_s = 0$,

$$\mathcal{V}_{(EW, Z_3)} = \mathcal{V}(r_1, r_2, s, \phi) \Big|_{r_1 = \frac{v_h}{\sqrt{2}}, r_2 = \frac{v_\Delta}{\sqrt{2}}, s = v_s, \phi = \frac{1}{3} \arccos(-1)} = 0. \tag{3.7}$$

2. ($r_1 \neq 0, s = 0$) vacuum: EW symmetry broken and Z_3 symmetry is retained with $v_h^2 \approx v_0^2, v_\Delta \approx 0, v_s = 0$,

$$\mathcal{V}_{(EW, Z_3)} = \mathcal{V}(r_1, r_2, s, \phi) \Big|_{r_1 = \frac{v_h}{\sqrt{2}}, r_2 = \frac{v_\Delta}{\sqrt{2}}, s = v_s, \phi = \frac{1}{3} \arccos(-1)} \approx -\frac{(M_h v_0)^2}{8}. \tag{3.8}$$

3. ($r_1 = 0, s \neq 0$) vacuum: Z_3 symmetry broken and EW symmetry is retained with the condition

$$v_h = v_\Delta = 0, v_s = \text{Root} \left[\frac{\partial \mathcal{V}(r_1, r_2, s, \phi)}{\partial s} \Big|_{r_1 = 0, r_2 = 0, \phi = \frac{1}{3} \arccos(-1)} = 0 \right]. \tag{3.9}$$

Here, the symbol Root denotes the solution of partial differential equation. Thus,

$$\mathcal{V}_{(EW, Z_3)} = \mathcal{V}(r_1, r_2, s, \phi) \Big|_{r_1 = \frac{v_h}{\sqrt{2}}, r_2 = \frac{v_\Delta}{\sqrt{2}}, s = v_s, \phi = \frac{1}{3} \arccos(-1)}. \tag{3.10}$$

4. ($r_1 \neq 0, s \neq 0$) vacuum: Breaking both EW and Z_3 symmetries with the condition

$$v_\Delta \approx 0, \begin{pmatrix} v_h \\ v_s \end{pmatrix} = \text{Root} \left[\left(\begin{array}{l} \left(\frac{\partial \mathcal{V}(r_1, r_2, s, \phi)}{\partial h} \Big|_{r_2 = 0, \phi = \frac{1}{3} \arccos(-1)} = 0 \right) \\ \left(\frac{\partial \mathcal{V}(r_1, r_2, s, \phi)}{\partial h = s} \Big|_{r_2 = 0, \phi = \frac{1}{3} \arccos(-1)} = 0 \right) \end{array} \right) \right]. \tag{3.11}$$

Thus,

$$\mathcal{V}_{(EW, Z_3)} = \mathcal{V}(r_1, r_2, s, \phi) \Big|_{r_1 = \frac{v_h}{\sqrt{2}}, r_2 = \frac{v_\Delta}{\sqrt{2}}, s = v_s, \phi = \frac{1}{3} \arccos(-1)}. \tag{3.12}$$

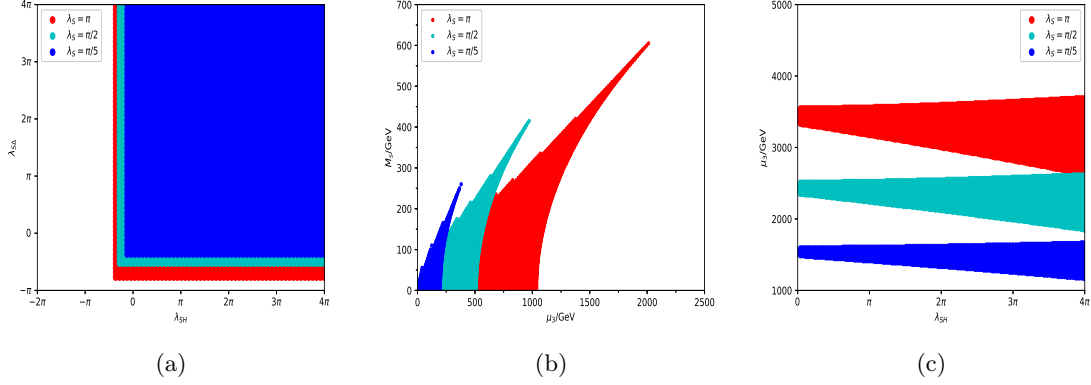


Figure 1: (a) The possible area in λ_{SH} vs $\lambda_{S\Delta}$ plane from perturbativity, perturbative unitary and vacuum stability by taking $\lambda_3 \approx \lambda_4 \approx 0$ and $\lambda_1 \approx \lambda_2 \approx \frac{2M_h^2}{v_0^2}$ at $\lambda_S = \pi, \pi/2, \pi/5$. (b) The possible area by requiring that \mathcal{V}_{EW,Z_3} vacuum is the expected SM one. (c) The possible area in $\lambda_{SH} - \mu_3$ plane with $M_S = 1$ TeV.

To ensure the condition that the vacuum value of \mathcal{V}_{EW,Z_3} is below the others, we need to estimate the values of Eq.(3.10) and Eq.(3.12) at given points $(M_S, \mu_3, \lambda_S, \lambda_{SH})$. We make a numerical scan in Figure 1. First, in Figure 1(a), we present the allowable area of λ_{SH} and $\lambda_{S\Delta}$ from perturbativity, perturbative unitary and vacuum stability constraints, by taking $\lambda_3 \simeq 0, \lambda_4 \simeq 0$ and $\lambda_1 = \lambda_2 \approx \frac{2m_h^2}{v_0^2}$. The red, green and blue areas correspond to λ_S equal $\pi, \pi/2$ and $\pi/5$, respectively. It is clear that the constraint of λ_{SH} and $\lambda_{S\Delta}$ from these conditions are weak. More, the allowable area is reduced as the value of λ_S becomes small. In the following, we take the region of $\lambda_{SH}, \lambda_{S\Delta} \in [0, 4\pi]$ to scan over. Then, in Figure 1(b) we present the scan area by requiring that \mathcal{V}_{EW,Z_3} vacuum is the expected SM one. The allowable region is restricted within the $\mu_3 - M_S$ plane. One comment is that, as M_S becomes larger, the solution of \mathcal{V}_{EW,Z_3} vacuum doesn't exist, due to at least one of the condition $v_s > 0, v_h^2 > 0, D_{EW,Z_3} \geq 0$ violates, where D_{EW,Z_3} is the discriminant of the quadratic form defined in Ref.[42]. Only values of \mathcal{V}_{EW,Z_3} and \mathcal{V}_{EW,Z_3} need to be compared with each other, result in a corresponding limitation on μ_3 . This can further be seen clearly in Figure 1(c) where we fix $M_S = 1$ TeV and vary μ_3 . The upper bounds express the maximum value of μ_3 meet the condition of $\mathcal{V}_{EW,Z_3} < \mathcal{V}_{EW,Z_3}$, and the lower boundary indicates the corresponding minimum value of μ_3 . Thus, the requirement that the SM vacuum is the the global minimum gives a limitation on the maximum value of μ_3 . As also can be seen in the figure, to obtain higher value of μ_3 , one prefers a larger value of λ_S .

4 Phenomenology

4.1 Relic density and Direct restriction

We are now considering the contribution of DM thermal cross sections to the relic abundance. There are mainly three ways of DM scattering that contribute: (a) annihilating to the SM particles; (b) annihilating to the triplet particles; (c) semi-annihilating to a dark matter and a Higgs particle. See Figure.2 for the illustrate channels in details.

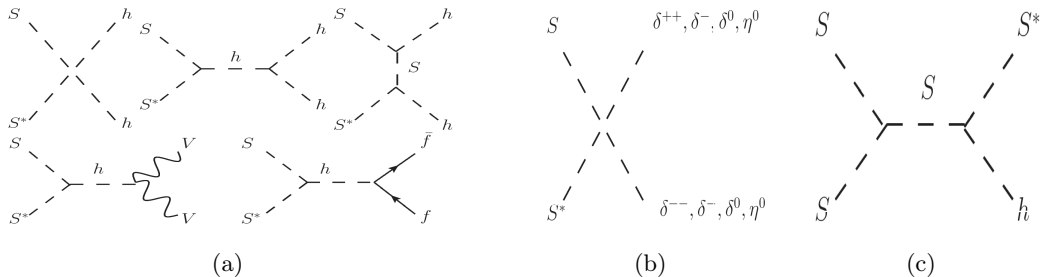


Figure 2: DM scattering Feynman diagrams of annihilating to the SM particles (a), triplet particles (b), and semi-annihilating to a dark matter and a Higgs particle (c).

The number density of the DM particles n satisfies the Boltzmann equation:

$$\begin{aligned} \frac{dn}{dt} - 3Hn &= -\langle\sigma v\rangle^{SS^*\rightarrow XX}(n^2 - \bar{n}^2) - \langle\sigma v\rangle^{SS^*\rightarrow\Delta\Delta}(n^2 - \bar{n}^2) \\ &\quad - \frac{1}{2}\langle\sigma v\rangle^{SS\rightarrow S^*h}(n^2 - n\bar{n}) \end{aligned} \quad (4.1)$$

where \bar{n} is the number density in thermal equilibrium, H is the Hubble expansion rate of the Universe, X denotes SM particles, Δ are the triplet particles ($\delta^{++(-)}, \delta^{+(-)}, \delta^0, \eta^0$), and $\langle\sigma v\rangle$ is the thermally averaged annihilation cross section, in terms of partial wave expansion $\langle\sigma v\rangle \simeq a + bv^2$. To distinguish different contributions of these three scattering channels on thermal cross section, we define the scattering cross section fraction N_i ($i = 1, 2, 3$) as:

$$N_1 = \frac{\frac{1}{2}\langle v\sigma\rangle^{SS\rightarrow S^*h}}{\langle v\sigma\rangle^{SS^*\rightarrow\Delta\Delta} + \langle v\sigma\rangle^{SS^*\rightarrow XX} + \frac{1}{2}\langle v\sigma\rangle^{SS\rightarrow S^*h}} \times 100\%, \quad (4.2)$$

$$N_2 = \frac{\langle v\sigma\rangle^{SS\rightarrow\Delta\Delta}}{\langle v\sigma\rangle^{SS^*\rightarrow\Delta\Delta} + \langle v\sigma\rangle^{SS^*\rightarrow XX} + \frac{1}{2}\langle v\sigma\rangle^{SS\rightarrow S^*h}} \times 100\%, \quad (4.3)$$

$$N_3 = (1 - N_1 - N_2). \quad (4.4)$$

Here N_3 denotes the fraction of DM pairs annihilating to SM particles. To calculate the DM relic density and the fraction N_i we use the micrOMGEAs5.0.6 package [71], in which the model has been implemented through the FeynRules package [72]. To constraint the parameter space, we require the relic density to fit the 2σ C.L. range of Planck result [14]: $\Omega_{DM}h^2 = 0.1199 \pm 0.0027$. The direct detection constraints is obtained from the spin-independent (SI) elastic scattering measurements. The SI elastic scattering cross section

function [47] is given by

$$\sigma_{SI} = \frac{\lambda_{SH}^2}{\pi M_H^4} \frac{M_N^2}{(M_N + M_S)^2} \times 0.0706 M_N^2, \quad (4.5)$$

where the nucleon mass $M_N \simeq 0.939$ GeV. The recent PandaX-II experiment [15] has given the upper limit of the SI elastic scattering cross section at a given DM mass M_S , which will lead to a maximum value of λ_{SH} . As N_1 is proportional to $\mu_3^2 \lambda_{SH}^2 / M_S^6$, in order to enhance the semi-annihilate contribution characterized by the Z_3 singlet scalar S , we choose $\lambda_S = \pi$ so that the parameter μ_3 is as larger as possible, while the condition that the (EW, Z_3) vacuum being the global minimum is still guaranteed, see in Figure 1(c) that has been discussed.

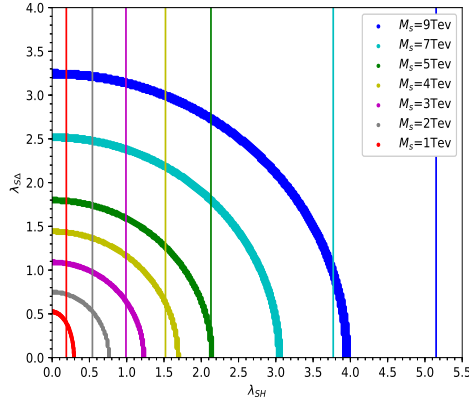


Figure 3: The allowable parameter space in λ_{SH} vs $\lambda_{S\Delta}$ plane adopting the requirement that the relic density should fit the Planck measurement in the 2σ C.L. range. The vertical line is the upper value of λ_{SH} at a given M_S based on PandaX-II measurements.

M_S [TeV]	λ_{SH}	$\lambda_{S\Delta}$	μ_3 [GeV]	N_1	N_2
1	0.19(PX.L.)	0.39	3544	24%	57%
2	0.54(PX.L.)	0.52	7089	12%	48%
3	0.99(PX.L.)	0.62	10637	8%	32%
4	1.52(PX.L.)	0.63	14179	6%	18%
5	2.13(PX.L.)	0~0.34	17724	5%	0%
7	3.07	0~0.20	24814	2%	0%
9	3.98	0~0.24	31904	2%	0%

Table 2: Benchmarks with the maximum λ_{SH} in Fig.(3). The symbol PX.L. denotes the PandaX-II limit.

A detailed scan is shown in Figure 3. As can be seen, we fix $M_\Delta = 0.9$ TeV while vary benchmark values of M_S that obey $M_S > M_\Delta$. Meanwhile, adopt the requirement that the

relic density should fit the Planck measurement in the 2σ C.L. range, the parameter space of λ_{SH} vs $\lambda_{S\Delta}$ is constrained within a quarter circle ring. Different ring relates to different choice of M_S . The vertical lines correspond to the PandaX-II measurements at a fixed M_Δ , clearly, as the DM mass M_S becomes larger, the upper boundary of λ_{SH} becomes larger correspondingly. The crossover point (or precisely, segment) of the same coloured ring and line, relates to a boundary point. The region on the left side of point fits both Planck as well as PandaX-II measurements, while the right side does not fit that of PandaX-II. With the increase of DM mass, the restriction of Planck experiment on λ_{SH} is more important than that of pandax-II. Notice when $M_S \geq 4$ TeV, the PandaX-II experiment would apply no constraints, only Planck results make sense.

More information at the crossover points is shown in Table 2. The second column is the upper boundary of λ_{SH} that fits both experiments. The upper values of μ_3 are also shown in the forth column, where the limits are set by the condition of $\mathcal{V}_{EW,Z_3} < \mathcal{V}_{EW,Z_3}$. The scattering cross section fractions are displayed in the last two columns. Though N_1 is proportional to $\mu_3^2 \lambda_{SH}^2$, it is inversely proportional to the sixth power of M_S , so that the maximum value of N_1 decreases significantly with the increase of M_S , even μ_3 increases.

4.2 Antiproton spectrum and electron-positron flux

The DM particles may annihilate to W and Z boson pairs through s-channel Higgs exchange. The subsequent decays of the bosons to antiproton will be responsible for the interpretation of the cosmic-ray antiprotons spectrum that has been measured by AMS [55], PAMELA [56] collaborations. On the other hand, the triplets produced from DM (co)annihilation may decay to leptons ($\Delta \rightarrow \ell^i \ell^j$) through Yukawa interactions, and is therefore possible to account for the excess of electron-positron flux in cosmic-ray exhibited in the AMS-02, Fermi-LAT, DAMPE experiments [43–45]. Notice the excess of positron-electron flux in cosmic-ray may also be explained by astrophysical evidence, for example, an isolated young pulsar [73]. Here in our paper, we focus on the DM interpretation and choose the DM mass at 3 TeV scale, which is large enough to produce the lepton with energy of the order of $\mathcal{O}(1)$ TeV. Following our above discussion, we choose $M_\Delta = 0.9$ TeV and $\mu_3 \approx 10$ TeV to enhance the semi-annihilation as so as possible. We focus on the parameter space where our model can give a nature DM explanation of both cosmic ray measurements as well as fit relic density measurement simultaneously, without negligible semi-annihilation effects.

To calculate the antiproton flux and electron-positron flux, we use the following parametrization functions [74–76]

$$\log_{10} \Phi_p^{bkg} = -1.64 + 0.07x - x^2 - 0.02x^3 + 0.028x^4, \quad (4.6)$$

$$\Phi_{e^-}^{prim}(E) = \frac{0.16E^{-1.1}}{1 + 11E^{0.9} + 3.2E^{2.15}} [GeV^{-1} cm^{-2} s^{-1} sr^{-1}], \quad (4.7)$$

$$\Phi_{e^-}^{sec}(E) = \frac{0.70E^{0.7}}{1 + 110E^{1.5} + 600E^{2.9} + 580E^{4.2}} [GeV^{-1} cm^{-2} s^{-1} sr^{-1}], \quad (4.8)$$

$$\Phi_{e^+}^{sec}(E) = \frac{4.5E^{0.7}}{1 + 650E^{2.3} + 1500E^{4.2}} [GeV^{-1} cm^{-2} s^{-1} sr^{-1}], \quad (4.9)$$

with $x = \log_{10} T/GeV$ in Eq.(4.6), the label $\Phi_{\bar{p}}^{bkg}$ denotes the cosmic-ray antiproton background. The label $\Phi^{prim(sec)}$ in Eq.(4.7)-Eq.(4.9) means the primary (secondary) cosmic of electron or positron background. The formula is appropriate for the energy range 10-1000 GeV [75]. The primary and secondary electron backgrounds are originated from supernova remnants and cosmic ray spallation in the interstellar medium, respectively. The secondary positrons background comes from primary protons colliding with other nuclei in the interstellar medium. With the value of BF mentioned above, the total antiproton and positron plus electron flux are given by:

$$\Phi_{\bar{p}} = \Phi_{\bar{p}}^{bkg} + BF \times \Phi_{\bar{p}}^{DM}. \quad (4.10)$$

$$\Phi_{e^+} + \Phi_{e^-} = k(\Phi_{e^-}^{(prim)} + \Phi_{e^-}^{(sec)} + \Phi_{e^+}^{(sec)}) + BF \times (\Phi_{e^-}^{DM} + \Phi_{e^+}^{DM}), \quad (4.11)$$

where k is the normalization parameter and we fix it as 0.9, Φ^{DM} is the corresponding flux from DM pair annihilation. The background fluxes can in principle be estimated. To calculate Φ^{DM} we use micrOMEGAs, in which the density distribution of DM in galactic halo is taken from Navarro-Frenk-White (NFW) density, and the effects of galactic charged particles propagation and solar modulation are considered.

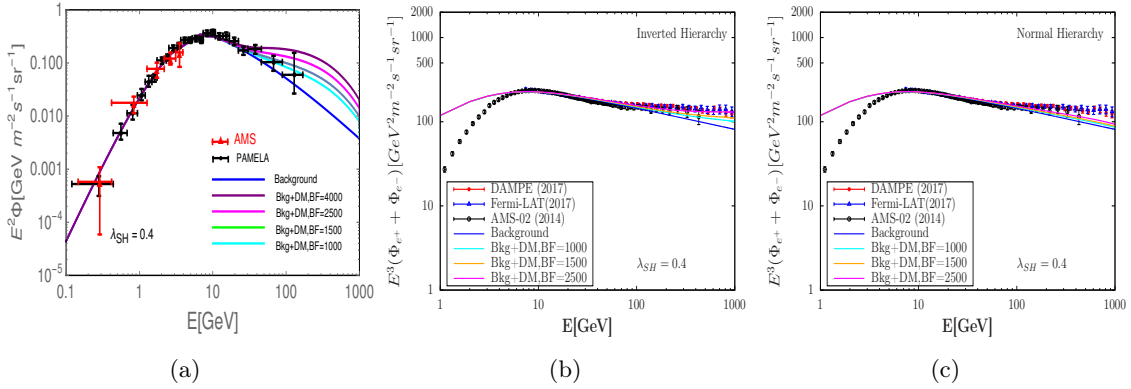


Figure 4: Background and background + DM (Bkg+DM) of cosmic-ray antiproton flux in (a), and electron-positron flux in (b) and (c) with inverted hierarchy (IH) and normal hierarchy (NH) scenario, respectively. The data points in (a) labels the PAMELA[56] and AMS[55] measurements. The data points in (b) and (c) stand for the AMS-02[43], Fermi-LAT[44] and DAMPE[45] measurements.

Considering the difference of the electron-positron spectrum between DAMPE and Fermi-LAT measurements when $E > 1$ TeV, we focus on the calculation of the flux when the value of E is located in the range of $0 \sim 1000$ GeV. The results of cosmic-ray antiproton as well as electron-positron fluxes are displayed in Figure 4 at $\lambda_{SH} = 0.4$ with different values of BF taken as free parameter. Figure 4(a) displays the background, background + DM (Bkg+DM) for $\Phi_{\bar{p}}$. Figure 4(b) and (c) show the background, background + DM (Bkg+DM) for $\Phi_{e^+} + \Phi_{e^-}$ in both IH and NH scenario, respectively. As can be seen in Figure 4(a), at a given value of $\lambda_{SH} = 0.4$, the PAMELA [56] results impose strong restriction on BF, where the maximum value is about 2500. Then in Figure 4(b) and (c), we keep the

same value of λ_{SH} , vary BF upto the maximum of 2500, and compare the positron-electron fluxes with DAMPE, Fermi-LAT, AMS-02 experiments. We find that, in the IH scenario, flux with small BF meets AMS and PAMELA results well while the DAMPE and Fermi-LAT experiments favor large values of BF. Select the appropriate BP value, we can fit all the experiment with our chosen parameters. Case is different for the NH scenario where the results only meet the AMS-02 measurements. There displays a suppression in the high E region. If we believe more in the results of DAMPE and Fermi-LAT experiment, the IH scenario is disfavored. The different behavior between these two scenarios is understood that, in our case, DM particles mainly annihilate into electron final states in the IH scenario rather than tau final states in the NH one. This can be seen directly from the final state decay fraction in Table 1, which is $e : \mu : \tau \approx 1 : 0.2 : 0.3$ for the IH scenario and $e : \mu : \tau \approx 1 : 0.5 : 1.4$ for that of NH.

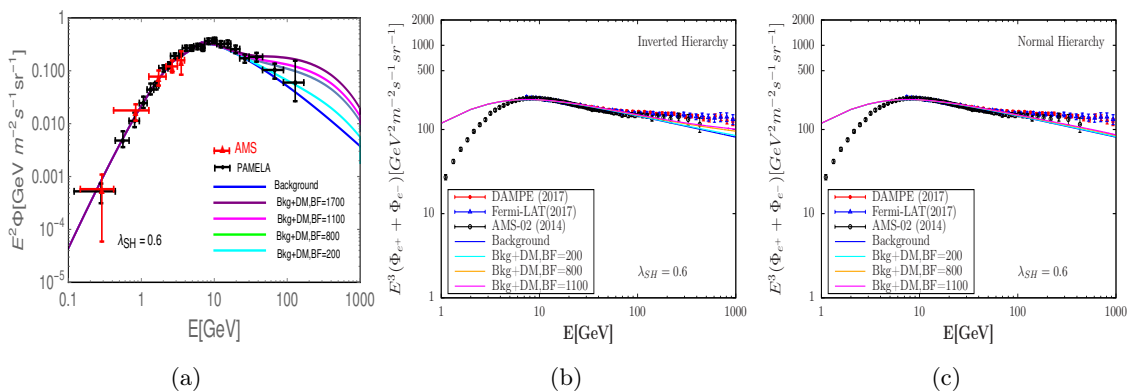


Figure 5: Same as Figure 4 but with $\lambda_{SH} = 0.6$.

We present a similar sector of figures in Figure 5, the only difference is $\lambda_{SH} = 0.6$. From Figure 5(a) we know that the maximum value BF is restricted to less than about 1100, otherwise it may lead to inappropriate antiproton spectrum measured by AMS. We then compare with the positron-electron flux, we find that neither IH nor NH scenario can meet the DAMPE and Fermi-LAT measurements. They can only meet AMS-02 experiment, and λ_{SH} should not be much higher. In fact the larger value of λ_{SH} is excluded by the AMS and PAMELA experiments, as in this case the triplet scalar productions are gradually reduced.

λ_{SH}	0.30	0.40	0.50	0.60	0.70
$\lambda_{S\Delta}$	1.04	1.01	0.98	0.95	0.88
N1	0%	1%	2%	3%	4%
N2	94%	90%	84%	76%	66%
BF	$\lesssim 4200$	$\lesssim 2500$	$\lesssim 1600$	$\lesssim 1100$	$\lesssim 800$

Table 3: The fraction scattering cross section N_i and maximum value of BFs at different values of $\lambda_{SH}/\lambda_{S\Delta}$.

We also select some feature points that meet the requirement of relic density, direct restriction, antiproton flux exhibited by AMS and PAMELA experimental results in Table 3. The fraction scattering cross section N_i and the maximum value of BF that allowable are shown, corresponding to different values of $\lambda_{SH}/\lambda_{S\Delta}$. We see that each value of λ_{SH} has an upper limit on BP. As λ_{SH} becomes larger, the BP value is reduced correspondingly, while the semi-annihilation contribution enhance, though only stand for a small fraction of the total. And small values of BF and $\lambda_{S\Delta}$ will also lead to bad fit to DAMPE and Fermi-LAT measurements. After the detailed analysis above, we get the conclusion that in order to meet appropriate antiproton spectrum and electron-positron flux, especially DAMPE and Fermi-LAT, we demand the value of λ_{SH} not large, i.e., smaller than 0.6. As a result, the fraction of semi-annihilation cross section is less than 3%.

N_1	λ_{SH}	$\lambda_{S\Delta}$	BF
1%	0.36	1.03	2600
2%	0.44	1.01	1900
3%	0.56	0.97	1500

Table 4: Benchmarks for fitting cosmic-ray antiproton flux and electron-positron flux.

To summary, we give some benchmarks listed in Table 4 which can fit the experiments well with $N_1 < 3\%$. The comparison with the experiments are present in Figure 6.

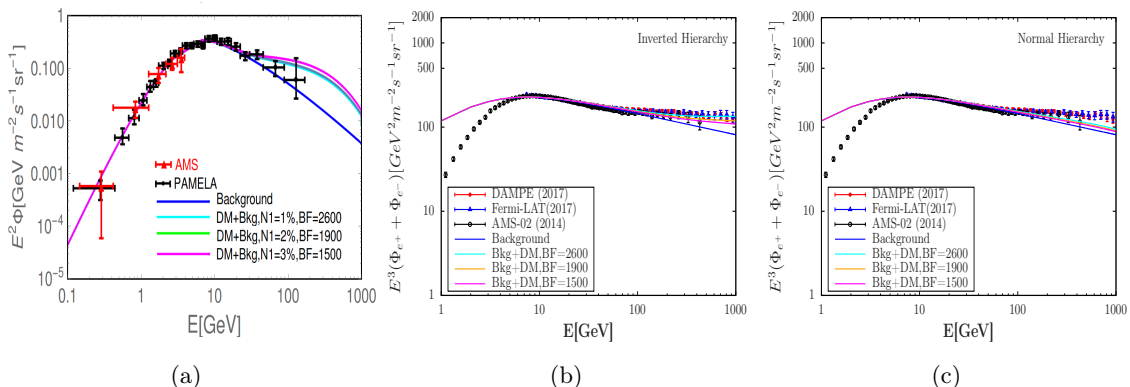


Figure 6: Background and background + DM (Bkg+DM) of cosmic-ray antiproton flux in (a), and electron-positron flux in (b) and (c) with inverted hierarchy (IH) and normal hierarchy (NH) scenario, respectively, with benchmarks list in Table 4. The data points in (a) labels the PAMELA[56] and AMS[55] measurements. The data points in (b) and (c) stand for the AMS-02[43], Fermi-LAT[44] and DAMPE[45] measurements.

5 Summary

The idea of combing Z_2 symmetry singlet scalar with Type-II Seesaw mechanism has been extensively studied in the literatures, see for example, Refs.[46, 77]. In this paper, we

combine the Type-II Seesaw mechanism with a complex singlet scalar of Z_3 symmetry to solve the origin of neutrino mass and dark matter beyond SM in one framework. The new cube term $S^3+S^{\dagger 3}$ would result in semi-annihilate effects contribute to Ωh^2 . We consider the dark matter in the heavy mass region ($M_S > M_\Delta$) and degenerate triplet scalar masses for numerical analysis. We find the constraints from perturbativity, perturbative unitarity and vacuum stability on λ_{SH} and $\lambda_{S\Delta}$ are weak. The Requirement that the $\mathcal{V}_{(EW,Z_3)}$ vacuum is the global minimum, or precisely, $\mathcal{V}_{(EW,Z_3)} < \mathcal{V}_{(EW,Z_3)}$, gives μ_3 a maximum value, which lead to the fact that the semi-annihilate process contribution fraction (N_1) has an upper limitation. We calculate the desirable area of λ_{SH} and $\lambda_{S\Delta}$ which are consistent with Planck and PandaX-II measurements at given values of M_Δ and M_S . As the dark mass M_S increases, the semi-annihilate process contribution fraction N_1 decreases gradually at the permissive maximum value of λ_{SH} and μ_3 .

When the triplets and the W, Z boson pairs produced from DM (co)annihilation, they will be responsible for the interpretation of the excess of electron-positron flux and antiproton spectrum with their subsequent decays. We alleviate the leptophilic properties of the DM to enhance the semi-annihilation effects and calculate those fluxes in both NH and IH scenarios. We find that, fitting the antiproton spectrum measured by AMS and PAMELA shows that the maximum value of BF decreases with the increase of λ_{SH} , and to fit the DAMPE and Fermi-LAT measurements one requires a large BF and small λ_{SH} . In order to fit simultaneously the electron-positron flux as well as the antiproton spectrum, strong restriction is set on the semi-annihilation cross section fraction (N_1), for example, for $M_S = 3$ TeV, N_1 should be less than 3%. No matter which case, the IH scenario is always the favored one.

Acknowledgments

The authors would like to thank Zhi-Long Han, Chuan-Hung Chen, and Takaaki Nomura for their useful and kind helps during technological implementation. Hao Sun is supported by the National Natural Science Foundation of China (Grant No. 12075043).

A Appendix

The first submatrix \mathcal{M}_1 of the scattering whose initial and final states have charge zero: $E_1 = (G^+\delta^-, \delta^+G^-, h\eta^0, \delta^0G^0, G^0\eta^0, h\delta^0, hs, \delta^0S, G^0S, \eta^0S, hS^*, \delta^0S^*, G^0S^*, \eta^0S^*)$. The first six states have discrete Z_3 symmetry with charge $X = 0$, and the last eight states

have $X = 2$. One can find:

$$\mathcal{M}_1 = \begin{pmatrix} \lambda_1 + \frac{\lambda_4}{2} & 0 & \frac{i\lambda_4}{2\sqrt{2}} & -\frac{i\lambda_4}{2\sqrt{2}} & \frac{\lambda_4}{2\sqrt{2}} & \frac{\lambda_4}{2\sqrt{2}} & 0 & 0 & 0 & 0 & 0 & 0 & 0 & 0 \\ 0 & \lambda_1 + \frac{\lambda_4}{2} & -\frac{i\lambda_4}{2\sqrt{2}} & \frac{i\lambda_4}{2\sqrt{2}} & \frac{\lambda_4}{2\sqrt{2}} & \frac{\lambda_4}{2\sqrt{2}} & 0 & 0 & 0 & 0 & 0 & 0 & 0 & 0 \\ \frac{i\lambda_4}{2\sqrt{2}} & -\frac{i\lambda_4}{2\sqrt{2}} & (\lambda_1 + \lambda_4) & 0 & 0 & 0 & 0 & 0 & 0 & 0 & 0 & 0 & 0 & 0 \\ -\frac{i\lambda_4}{2\sqrt{2}} & \frac{i\lambda_4}{2\sqrt{2}} & 0 & \lambda_1 + \lambda_4 & 0 & 0 & 0 & 0 & 0 & 0 & 0 & 0 & 0 & 0 \\ \frac{\lambda_4}{2\sqrt{2}} & \frac{\lambda_4}{2\sqrt{2}} & 0 & 0 & \lambda_1 + \lambda_4 & 0 & 0 & 0 & 0 & 0 & 0 & 0 & 0 & 0 \\ \frac{\lambda_4}{2\sqrt{2}} & \frac{\lambda_4}{2\sqrt{2}} & 0 & 0 & 0 & \lambda_1 + \lambda_4 & 0 & 0 & 0 & 0 & 0 & 0 & 0 & 0 \\ 0 & 0 & 0 & 0 & 0 & 0 & \lambda_{SH} & 0 & 0 & 0 & 0 & 0 & 0 & 0 \\ 0 & 0 & 0 & 0 & 0 & 0 & 0 & \lambda_{S\Delta} & 0 & 0 & 0 & 0 & 0 & 0 \\ 0 & 0 & 0 & 0 & 0 & 0 & 0 & 0 & \lambda_{SH} & 0 & 0 & 0 & 0 & 0 \\ 0 & 0 & 0 & 0 & 0 & 0 & 0 & 0 & 0 & \lambda_{S\Delta} & 0 & 0 & 0 & 0 \\ 0 & 0 & 0 & 0 & 0 & 0 & 0 & 0 & 0 & 0 & \lambda_{SH} & 0 & 0 & 0 \\ 0 & 0 & 0 & 0 & 0 & 0 & 0 & 0 & 0 & 0 & 0 & \lambda_{S\Delta} & 0 & 0 \\ 0 & 0 & 0 & 0 & 0 & 0 & 0 & 0 & 0 & 0 & 0 & 0 & \lambda_{SH} & 0 \\ 0 & 0 & 0 & 0 & 0 & 0 & 0 & 0 & 0 & 0 & 0 & 0 & 0 & \lambda_{S\Delta} \end{pmatrix}. \quad (\text{A.1})$$

The second submatrix \mathcal{M}_2 of the scattering whose initial and final states have charge zero: $E_2 = (G^+G^-, \delta^+\delta^-, \frac{G^0G^0}{\sqrt{2}}, \frac{\eta^0\eta^0}{\sqrt{2}}, \frac{h\bar{h}}{2}, \frac{\delta^0\delta^0}{\sqrt{2}}, \delta^{++}\delta^{--}, SS^*)$. All these states have discrete Z_3 charge $X = 0$. One can find:

$$\mathcal{M}_2 = \begin{pmatrix} 4\lambda & \lambda_1 + \frac{\lambda_4}{2} & \frac{4\lambda}{2\sqrt{2}} & \frac{\lambda_1}{\sqrt{2}} & \frac{4\lambda}{2\sqrt{2}} & \frac{\lambda_1}{\sqrt{2}} & \lambda_1 + \lambda_4 & \lambda_{SH} \\ \lambda_1 + \frac{\lambda_4}{2} & 4\lambda_2 + 2\lambda_3 & \frac{2\lambda_1 + \lambda_4}{2\sqrt{2}} & \sqrt{2}(\lambda_2 + \lambda_3) & \frac{2\lambda_1 + \lambda_4}{2\sqrt{2}} & \sqrt{2}(\lambda_2 + \lambda_3) & 2(\lambda_2 + \lambda_3) & \lambda_{S\Delta} \\ \frac{4\lambda}{2\sqrt{2}} & \frac{2\lambda_1 + \lambda_4}{2\sqrt{2}} & 3\lambda & \frac{\lambda_1 + \lambda_4}{2} & \lambda & \frac{\lambda_1 + \lambda_4}{2} & \frac{\lambda_1}{\sqrt{2}} & \frac{\lambda_{SH}}{\sqrt{2}} \\ \frac{\lambda_1}{\sqrt{2}} & \sqrt{2}(\lambda_2 + \lambda_3) & \frac{\lambda_1 + \lambda_4}{2} & 3(\lambda_2 + \lambda_3) & \frac{\lambda_1 + \lambda_4}{2} & (\lambda_2 + \lambda_3) & \sqrt{2}\lambda_2 & \frac{\lambda_{S\Delta}}{\sqrt{2}} \\ \frac{4\lambda}{2\sqrt{2}} & \frac{2\lambda_1 + \lambda_4}{2\sqrt{2}} & \lambda & \frac{\lambda_1 + \lambda_4}{2} & 3\lambda & \frac{\lambda_1 + \lambda_4}{2} & \frac{\lambda_1}{\sqrt{2}} & \frac{\lambda_{SH}}{\sqrt{2}} \\ \frac{\lambda_1}{\sqrt{2}} & \sqrt{2}(\lambda_2 + \lambda_3) & \frac{\lambda_1 + \lambda_4}{2} & (\lambda_2 + \lambda_3) & \frac{\lambda_1 + \lambda_4}{2} & 3(\lambda_2 + \lambda_3) & \sqrt{2}\lambda_2 & \frac{\lambda_{S\Delta}}{\sqrt{2}} \\ (\lambda_1 + \lambda_4) & 2(\lambda_2 + \lambda_3) & \frac{\lambda_1}{\sqrt{2}} & \sqrt{2}\lambda_2 & \frac{\lambda_1}{\sqrt{2}} & \sqrt{2}\lambda_2 & 4(\lambda_2 + \lambda_3) & \lambda_{S\Delta} \\ \lambda_{SH} & \lambda_{S\Delta} & \frac{\lambda_{SH}}{\sqrt{2}} & \frac{\lambda_{S\Delta}}{\sqrt{2}} & \frac{\lambda_{SH}}{\sqrt{2}} & \frac{\lambda_{S\Delta}}{\sqrt{2}} & \lambda_{S\Delta} & 4\lambda_S \end{pmatrix}. \quad (\text{A.2})$$

The third submatrix \mathcal{M}_3 of the scattering whose initial and final states have charge zero: $E_3 = (hG^0, \delta^0\eta^0, \frac{SS}{\sqrt{2}}, \frac{S^*S^*}{\sqrt{2}})$. The first two states have discrete Z_3 charge $X = 0$, the states $\frac{S^*S^*}{\sqrt{2}}$ and $\frac{SS}{\sqrt{2}}$ have $X = 2$ and $X = 1$ respectively. One can find:

$$\mathcal{M}_3 = \begin{pmatrix} 2\lambda & 0 & 0 & 0 \\ 0 & 2(\lambda_2 + \lambda_3) & 0 & 0 \\ 0 & 0 & \lambda_S & 0 \\ 0 & 0 & 0 & \lambda_S \end{pmatrix}. \quad (\text{A.3})$$

The fourth submatrix \mathcal{M}_4 of the scattering whose initial and final states are charge one: $E_4 = (hG^+, \delta^0G^+, G^0G^+, \eta^0G^+, h\delta^+, \delta^0\delta^+, G^0\delta^+, \eta^0\delta^+, \delta^{++}\delta^-, \delta^{++}G^-, SG^+, S\delta^+, S^*G^+, S^*\delta^+)$. The first ten states have discrete Z_3 charge $X = 0$, the states $SG^+, S\delta^+$ and

$S^*G^+, S^*\delta^+$ have $X = 1$ and $X = 2$ respectively. One can find:

$$\mathcal{M}_4 = \begin{pmatrix} 2\lambda & 0 & 0 & 0 & 0 & \frac{\lambda_4}{2\sqrt{2}} & 0 & -i\frac{\lambda_4}{2\sqrt{2}} & -\frac{\lambda_4}{2} & 0 & 0 & 0 & 0 & 0 \\ 0 & \lambda_1 & 0 & 0 & \frac{\lambda_4}{2\sqrt{2}} & 0 & i\frac{\lambda_4}{2\sqrt{2}} & 0 & 0 & 0 & 0 & 0 & 0 & 0 \\ 0 & 0 & 2\lambda & 0 & 0 & i\frac{\lambda_4}{2\sqrt{2}} & 0 & \frac{\lambda_4}{2\sqrt{2}} & -i\frac{\lambda_4}{2} & 0 & 0 & 0 & 0 & 0 \\ 0 & 0 & 0 & \lambda_1 & -i\frac{\lambda_4}{2\sqrt{2}} & 0 & \frac{\lambda_4}{2\sqrt{2}} & 0 & 0 & 0 & 0 & 0 & 0 & 0 \\ 0 & \frac{\lambda_4}{2\sqrt{2}} & 0 & -\frac{\lambda_4}{2\sqrt{2}} & \frac{2\lambda_1 + \lambda_4}{2} & 0 & 0 & 0 & 0 & -\frac{\lambda_4}{2} & 0 & 0 & 0 & 0 \\ \frac{\lambda_4}{2\sqrt{2}} & 0 & i\frac{\lambda_4}{2\sqrt{2}} & 0 & 0 & 2(\lambda_2 + \lambda_3) & 0 & 0 & -\sqrt{2}\lambda_3 & 0 & 0 & 0 & 0 & 0 \\ 0 & i\frac{\lambda_4}{2\sqrt{2}} & 0 & \frac{\lambda_4}{2\sqrt{2}} & 0 & 0 & \frac{2\lambda_1 + \lambda_4}{2} & 0 & 0 & -i\frac{\lambda_4}{2} & 0 & 0 & 0 & 0 \\ -i\frac{\lambda_4}{2\sqrt{2}} & 0 & \frac{\lambda_4}{2\sqrt{2}} & 0 & 0 & 0 & 0 & 2(\lambda_2 + \lambda_3) & -i\sqrt{2}\lambda_3 & 0 & 0 & 0 & 0 & 0 \\ -\frac{\lambda_4}{2} & 0 & -i\frac{\lambda_4}{2} & 0 & 0 & -\sqrt{2}\lambda_3 & 0 & -i\sqrt{2}\lambda_3 & 2(\lambda_2 + \lambda_3) & 0 & 0 & 0 & 0 & 0 \\ 0 & 0 & 0 & 0 & -\frac{\lambda_4}{2} & 0 & -i\frac{\lambda_4}{2} & 0 & 0 & \lambda_1 + \lambda_4 & 0 & 0 & 0 & 0 \\ 0 & 0 & 0 & 0 & 0 & 0 & 0 & 0 & 0 & 0 & \lambda_{SH} & 0 & 0 & 0 \\ 0 & 0 & 0 & 0 & 0 & 0 & 0 & 0 & 0 & 0 & 0 & \lambda_{S\Delta} & 0 & 0 \\ 0 & 0 & 0 & 0 & 0 & 0 & 0 & 0 & 0 & 0 & 0 & 0 & \lambda_{SH} & 0 \\ 0 & 0 & 0 & 0 & 0 & 0 & 0 & 0 & 0 & 0 & 0 & 0 & 0 & \lambda_{S\Delta} \end{pmatrix}. \quad (\text{A.4})$$

The fifth submatrix \mathcal{M}_5 of the scattering whose initial and final states have charge two: $E_5 = (G^+G^+, \frac{\delta^+\delta^+}{\sqrt{2}}, \delta^+G^+, \delta^{++}\delta^0, \delta^{++}\eta^0, \delta^{++}G^0, \delta^{++}h, \delta^{++}S, \delta^{++}S^*)$. The first seven states have discrete Z_3 charge $X = 0$, the states $\delta^{++}S$ and $\delta^{++}S^*$ have $X = 1$ and $X = 2$ respectively. One can find:

$$\mathcal{M}_5 = \begin{pmatrix} 2\lambda & 0 & 0 & 0 & 0 & 0 & 0 & 0 & 0 & 0 \\ 0 & 2\lambda_2 + \lambda_3 & 0 & -\lambda_3 & -i\lambda_3 & 0 & 0 & 0 & 0 & 0 \\ 0 & 0 & \frac{2\lambda_1 + \lambda_4}{2} & 0 & 0 & -i\frac{\lambda_4}{2} & -\frac{\lambda_4}{2} & 0 & 0 & 0 \\ 0 & -\lambda_3 & 0 & 2\lambda_2 & 0 & 0 & 0 & 0 & 0 & 0 \\ 0 & -i\lambda_3 & 0 & 0 & 2\lambda_2 & 0 & 0 & 0 & 0 & 0 \\ 0 & 0 & -i\frac{\lambda_4}{2} & 0 & 0 & \lambda_1 & 0 & 0 & 0 & 0 \\ 0 & 0 & -\frac{\lambda_4}{2} & 0 & 0 & 0 & \lambda_1 & 0 & 0 & 0 \\ 0 & 0 & 0 & 0 & 0 & 0 & 0 & \lambda_{S\Delta} & 0 & 0 \\ 0 & 0 & 0 & 0 & 0 & 0 & 0 & 0 & 0 & \lambda_{SH} \end{pmatrix}. \quad (\text{A.5})$$

The sixth submatrix \mathcal{M}_6 of the scattering whose initial and final states have charge three: $E_6 = (\delta^{++}G^+, \delta^{++}\delta^+)$. All states have discrete Z_3 charge $X = 0$. One can find:

$$\mathcal{M}_6 = \begin{pmatrix} \lambda_1 + \lambda_4 & 0 \\ 0 & 2(\lambda_2 + \lambda_3) \end{pmatrix}. \quad (\text{A.6})$$

The last submatrix \mathcal{M}_7 of the scattering whose initial and final states have charge four: $E_7 = \frac{\delta^{++}\delta^{++}}{\sqrt{2}}$, its discrete Z_3 charge $X = 0$. The \mathcal{M}_7 is $2(\lambda_2 + \lambda_3)$.

The eigenvalues e_i^j of the submatrix \mathcal{M}_i can be written as

$$\begin{aligned}
e_1^1 &= \lambda_1 + \lambda_4, e_1^2 = \lambda_1, e_1^3 = \lambda_1 + \frac{3}{2}\lambda_4, e_1^4 = \lambda_{SH}, \\
e_1^5 &= \lambda_{S\Delta}, e_2^1 = 2\lambda, e_2^2 = 2\lambda_2, e_2^3 = 2(\lambda_2 + \lambda_3), \\
e_2^4 &= \lambda + \lambda_2 + 2\lambda_3 + \sqrt{\lambda^2 - 2\lambda\lambda_2 + \lambda_2^2 - 4\lambda\lambda_3 + 4\lambda_2\lambda_3 + 4\lambda_3^2 + \lambda_4^2}, \\
e_2^5 &= \lambda + \lambda_2 + 2\lambda_3 - \sqrt{\lambda^2 - 2\lambda\lambda_2 + \lambda_2^2 - 4\lambda\lambda_3 + 4\lambda_2\lambda_3 + 4\lambda_3^2 + \lambda_4^2}, \\
e_2^6 &= \frac{1}{4}\text{Root}[A], e_3^1 = 2\lambda, e_3^2 = 2(\lambda_2 + \lambda_3), e_3^3 = \lambda_S, e_4^1 = \lambda_1 + \lambda_4, e_4^2 = \lambda_1, \\
e_4^3 &= \lambda_1 + \frac{3\lambda_4}{2}, e_4^4 = 2\lambda, e_4^5 = 2\lambda_2, e_4^6 = 2(\lambda_2 + \lambda_3), e_4^7 = \lambda_1 - \frac{\lambda_4}{2}, \\
e_4^8 &= \frac{1}{4}[4\lambda + 4\lambda_2 + 8\lambda_3 + \sqrt{(4\lambda - 4\lambda_2 - 8\lambda_3)^2 + 16\lambda_4^2}], \\
e_4^9 &= \frac{1}{4}[4\lambda + 4\lambda_2 + 8\lambda_3 - \sqrt{(4\lambda - 4\lambda_2 - 8\lambda_3)^2 + 16\lambda_4^2}], \\
e_4^{10} &= \lambda_{SH}, e_4^{11} = \lambda_{S\Delta}, e_5^1 = \lambda_1 + \lambda_4, e_5^2 = \lambda_1, e_5^3 = 2\lambda, e_5^4 = 2\lambda_2, e_5^5 = 2(\lambda_2 + \lambda_3), \\
e_5^6 &= \lambda_1 - \frac{\lambda_4}{2}, e_5^7 = 2\lambda_2 - \lambda_3, e_5^8 = \lambda_{S\Delta}, e_6^1 = \lambda_1 + \lambda_4, e_6^2 = 2(\lambda_2 + \lambda_3), e_6^3 = 2(\lambda_2 + \lambda_3).
\end{aligned} \tag{A.7}$$

Where we have ignored duplicate eigenvalues for \mathcal{M}_i . The symbol $\text{Root}[A]$ stand for the roots of cubic equation, we will apply Samuelson's inequality [78] to place restrictions on the region of roots.

$$\begin{aligned}
&x^3 + x^2(-24\lambda - 32\lambda_2 - 24\lambda_3 - 16\lambda_S) + x(-96\lambda_1^2 + 768\lambda\lambda_2 + 576\lambda\lambda_3 - 100\lambda_1\lambda_4 - 26\lambda_4^2) \\
&+ 1536\lambda_1^2\lambda_S - 12288\lambda\lambda_2\lambda_S - 9216\lambda\lambda_3\lambda_S + 1600\lambda_1\lambda_4\lambda_S + 416\lambda_4^2\lambda_S + 1152\lambda\lambda_{S\Delta} \\
&- 768\lambda_1\lambda_{S\Delta}\lambda_{SH} - 400\lambda_4\lambda_{S\Delta}\lambda_{SH} + 1024\lambda_2\lambda_{SH}^2 + 768\lambda_3\lambda_{SH}^2 = 0.
\end{aligned} \tag{A.8}$$

References

- [1] F. Zwicky, *Die Rotverschiebung von extragalaktischen Nebeln*, *Helv. Phys. Acta* **6** (1933) 110–127.
- [2] S. W. Allen, A. E. Evrard, and A. B. Mantz, *Cosmological Parameters from Observations of Galaxy Clusters*, *Ann. Rev. Astron. Astrophys.* **49** (2011) 409–470, [[arXiv:1103.4829](#)].
- [3] V. C. Rubin, N. Thonnard, and W. K. Ford, Jr., *Rotational properties of 21 SC galaxies with a large range of luminosities and radii, from NGC 4605 /R = 4kpc/ to UGC 2885 /R = 122 kpc/*, *Astrophys. J.* **238** (1980) 471.
- [4] C. S. Frenk and S. D. M. White, *Dark matter and cosmic structure*, *Annalen Phys.* **524** (2012) 507–534, [[arXiv:1210.0544](#)].
- [5] A. Refregier, *Weak gravitational lensing by large scale structure*, *Ann. Rev. Astron. Astrophys.* **41** (2003) 645–668, [[astro-ph/0307212](#)].
- [6] **WMAP** Collaboration, G. Hinshaw et al., *Nine-Year Wilkinson Microwave Anisotropy Probe (WMAP) Observations: Cosmological Parameter Results*, *Astrophys. J. Suppl.* **208** (2013) 19, [[arXiv:1212.5226](#)].

- [7] K. A. O. E. Al., *Review of particle physics*, *Chinese Physics C* (2014).
- [8] S.-M. Choi and H. M. Lee, *SIMP dark matter with gauged Z_3 symmetry*, *JHEP* **09** (2015) 063, [[arXiv:1505.00960](#)].
- [9] Y. Hochberg, E. Kuflik, T. Volansky, and J. G. Wacker, *Mechanism for Thermal Relic Dark Matter of Strongly Interacting Massive Particles*, *Phys. Rev. Lett.* **113** (2014) 171301, [[arXiv:1402.5143](#)].
- [10] Y. Hochberg, E. Kuflik, H. Murayama, T. Volansky, and J. G. Wacker, *Model for Thermal Relic Dark Matter of Strongly Interacting Massive Particles*, *Phys. Rev. Lett.* **115** (2015), no. 2 021301, [[arXiv:1411.3727](#)].
- [11] H. M. Lee and M.-S. Seo, *Communication with SIMP dark mesons via Z' -portal*, *Phys. Lett. B* **748** (2015) 316–322, [[arXiv:1504.00745](#)].
- [12] S.-M. Choi, Y.-J. Kang, and H. M. Lee, *On thermal production of self-interacting dark matter*, *JHEP* **12** (2016) 099, [[arXiv:1610.04748](#)].
- [13] R. T. D’Agnolo and J. T. Ruderman, *Light Dark Matter from Forbidden Channels*, *Phys. Rev. Lett.* **115** (2015), no. 6 061301, [[arXiv:1505.07107](#)].
- [14] **Planck** Collaboration, P. A. R. Ade et al., *Planck 2015 results. XIII. Cosmological parameters*, *Astron. Astrophys.* **594** (2016) A13, [[arXiv:1502.01589](#)].
- [15] **PandaX-II** Collaboration, X. Cui et al., *Dark Matter Results From 54-Ton-Day Exposure of PandaX-II Experiment*, *Phys. Rev. Lett.* **119** (2017), no. 18 181302, [[arXiv:1708.06917](#)].
- [16] P. Minkowski, *$\mu \rightarrow e\gamma$ at a Rate of One Out of 10^9 Muon Decays?*, *Phys. Lett. B* **67** (1977) 421–428.
- [17] T. Yanagida, *in Proceedings of the Workshop on the Baryon Number of the Universe and Unified Theories, Tsukuba, Japan, 13-14 Feb 1979, O.Sawada and A.Sugamoto (eds.), KEK report KEK-79-18* (1979) p.95.
- [18] R. N. Mohapatra and G. Senjanovic, *Neutrino Mass and Spontaneous Parity Nonconservation*, *Phys. Rev. Lett.* **44** (1980) 912.
- [19] M. Magg and C. Wetterich, *Neutrino Mass Problem and Gauge Hierarchy*, *Phys. Lett. B* **94** (1980) 61–64.
- [20] G. Lazarides, Q. Shafi, and C. Wetterich, *Proton Lifetime and Fermion Masses in an $SO(10)$ Model*, *Nucl. Phys. B* **181** (1981) 287–300.
- [21] D. Ashery, I. Navon, G. Azuelos, H. K. Walter, H. J. Pfeiffer, and F. W. Schleputz, *True Absorption and Scattering of Pions on Nuclei*, *Phys. Rev. C* **23** (1981) 2173–2185.
- [22] E. Ma and U. Sarkar, *Neutrino masses and leptogenesis with heavy Higgs triplets*, *Phys. Rev. Lett.* **80** (1998) 5716–5719, [[hep-ph/9802445](#)].
- [23] W. Konetschny and W. Kummer, *Nonconservation of Total Lepton Number with Scalar Bosons*, *Phys. Lett. B* **70** (1977) 433–435.
- [24] J. Schechter and J. W. F. Valle, *Neutrino Masses in $SU(2) \times U(1)$ Theories*, *Phys. Rev. D* **22** (1980) 2227.
- [25] T. P. Cheng and L.-F. Li, *Neutrino Masses, Mixings and Oscillations in $SU(2) \times U(1)$ Models of Electroweak Interactions*, *Phys. Rev. D* **22** (1980) 2860.

- [26] S. M. Bilenky, J. Hosek, and S. T. Petcov, *On Oscillations of Neutrinos with Dirac and Majorana Masses*, *Phys. Lett. B* **94** (1980) 495–498.
- [27] Ma and Ernest, *Pathways to naturally small neutrino masses*, *Physical Review Letters* **81** (1998), no. 6 1171–1174.
- [28] B. Bajc and G. Senjanovi?, *Seesaw at lhc*, *Journal of High Energy Physics* (2006), no. 12.
- [29] P. F. Pérez, *Renormalizable adjoint $su(5)$* , *Physics Letters B* **654** (2007), no. 5 189–193.
- [30] P. Fileviez Perez, *Supersymmetric Adjoint $SU(5)$* , *Phys. Rev. D* **76** (2007) 071701, [[arXiv:0705.3589](#)].
- [31] N. G. Deshpande and E. Ma, *Pattern of symmetry breaking with two higgs doublets*, *Physical review D: Particles and fields* **18:7** (1978), no. 7 2574–2576.
- [32] E. Ma, *Verifiable radiative seesaw mechanism of neutrino mass and dark matter*, *Phys. Rev. D* **73** (2006) 077301, [[hep-ph/0601225](#)].
- [33] R. Barbieri, L. J. Hall, and V. S. Rychkov, *Improved naturalness with a heavy Higgs: An Alternative road to LHC physics*, *Phys. Rev. D* **74** (2006) 015007, [[hep-ph/0603188](#)].
- [34] L. Lopez Honorez, E. Nezri, J. F. Oliver, and M. H. G. Tytgat, *The Inert Doublet Model: An Archetype for Dark Matter*, *JCAP* **02** (2007) 028, [[hep-ph/0612275](#)].
- [35] G. Bélanger, K. Kannike, A. Pukhov, and M. Raidal, *Minimal semi-annihilating \mathbb{Z}_N scalar dark matter*, *JCAP* **06** (2014) 021, [[arXiv:1403.4960](#)].
- [36] G. Belanger, K. Kannike, A. Pukhov, and M. Raidal, *Impact of semi-annihilations on dark matter phenomenology - an example of Z_N symmetric scalar dark matter*, *JCAP* **04** (2012) 010, [[arXiv:1202.2962](#)].
- [37] S. P. Martin, *Some simple criteria for gauged R -parity*, *Phys. Rev. D* **46** (1992) 2769–2772, [[hep-ph/9207218](#)].
- [38] L. M. Krauss and F. Wilczek, *Discrete Gauge Symmetry in Continuum Theories*, *Phys. Rev. Lett.* **62** (1989) 1221.
- [39] P. Ko and Y. Tang, *Self-interacting scalar dark matter with local Z_3 symmetry*, *JCAP* **05** (2014) 047, [[arXiv:1402.6449](#)].
- [40] N. Bernal, C. Garcia-Cely, and R. Rosenfeld, *WIMP and SIMP Dark Matter from the Spontaneous Breaking of a Global Group*, *JCAP* **04** (2015) 012, [[arXiv:1501.01973](#)].
- [41] A. Hektor, A. Hryczuk, and K. Kannike, *Improved bounds on \mathbb{Z}_3 singlet dark matter*, *JHEP* **03** (2019) 204, [[arXiv:1901.08074](#)].
- [42] G. Belanger, K. Kannike, A. Pukhov, and M. Raidal, *Z_3 Scalar Singlet Dark Matter*, *JCAP* **01** (2013) 022, [[arXiv:1211.1014](#)].
- [43] **AMS** Collaboration, M. Aguilar et al., *Electron and Positron Fluxes in Primary Cosmic Rays Measured with the Alpha Magnetic Spectrometer on the International Space Station*, *Phys. Rev. Lett.* **113** (2014) 121102.
- [44] **Fermi-LAT** Collaboration, S. Abdollahi et al., *Cosmic-ray electron-positron spectrum from 7 GeV to 2 TeV with the Fermi Large Area Telescope*, *Phys. Rev. D* **95** (2017), no. 8 082007, [[arXiv:1704.07195](#)].
- [45] **DAMPE** Collaboration, G. Ambrosi et al., *Direct detection of a break in the teraelectronvolt*

- cosmic-ray spectrum of electrons and positrons*, *Nature* **552** (2017) 63–66, [[arXiv:1711.10981](#)].
- [46] P. S. B. Dev, D. K. Ghosh, N. Okada, and I. Saha, *Neutrino Mass and Dark Matter in light of recent AMS-02 results*, *Phys. Rev. D* **89** (2014) 095001, [[arXiv:1307.6204](#)].
- [47] T. Li, N. Okada, and Q. Shafi, *Scalar dark matter, Type II Seesaw and the DAMPE cosmic ray $e^+ + e^-$ excess*, *Phys. Lett. B* **779** (2018) 130–135, [[arXiv:1712.00869](#)].
- [48] T. Li, N. Okada, and Q. Shafi, *Type II seesaw mechanism with scalar dark matter in light of AMS-02, DAMPE, and Fermi-LAT data*, *Phys. Rev. D* **98** (2018), no. 5 055002, [[arXiv:1804.09835](#)].
- [49] H. Motz, H. Okada, Y. Asaoka, and K. Kohri, *Cosmic-ray signatures of dark matter from a flavor dependent gauge symmetry model with neutrino mass mechanism*, *Phys. Rev. D* **102** (2020), no. 8 083019, [[arXiv:2004.04304](#)].
- [50] J. Cao, X. Guo, L. Shang, F. Wang, P. Wu, and L. Zu, *Scalar dark matter explanation of the DAMPE data in the minimal Left-Right symmetric model*, *Phys. Rev. D* **97** (2018), no. 6 063016, [[arXiv:1712.05351](#)].
- [51] G. Beck, M. Kumar, E. Malwa, B. Mellado, and R. Temo, *Connecting multi-lepton anomalies at the LHC and in Astrophysics and the prospects of MeerKAT/SKA*, **2**, 2021. [[arXiv:2102.10596](#)].
- [52] M. Ibe, H. Murayama, and T. T. Yanagida, *Breit-Wigner Enhancement of Dark Matter Annihilation*, *Phys. Rev. D* **79** (2009) 095009, [[arXiv:0812.0072](#)].
- [53] J. D. March-Russell and S. M. West, *WIMPonium and Boost Factors for Indirect Dark Matter Detection*, *Phys. Lett. B* **676** (2009) 133–139, [[arXiv:0812.0559](#)].
- [54] W.-L. Guo and Y.-L. Wu, *Enhancement of Dark Matter Annihilation via Breit-Wigner Resonance*, *Phys. Rev. D* **79** (2009) 055012, [[arXiv:0901.1450](#)].
- [55] **AMS** Collaboration, M. Aguilar et al., *The Alpha Magnetic Spectrometer (AMS) on the International Space Station. I: Results from the test flight on the space shuttle*, *Phys. Rept.* **366** (2002) 331–405. [Erratum: *Phys.Rept.* 380, 97–98 (2003)].
- [56] **PAMELA** Collaboration, O. Adriani et al., *PAMELA results on the cosmic-ray antiproton flux from 60 MeV to 180 GeV in kinetic energy*, *Phys. Rev. Lett.* **105** (2010) 121101, [[arXiv:1007.0821](#)].
- [57] C. Patrignani, *Review of particle physics*, *Physics Letters B* **40** (2016), no. 10 1–4.
- [58] C.-H. Chen and T. Nomura, *Inert Dark Matter in Type-II Seesaw*, *JHEP* **09** (2014) 120, [[arXiv:1404.2996](#)].
- [59] I. Esteban, M. C. Gonzalez-Garcia, M. Maltoni, I. Martinez-Soler, and T. Schwetz, *Updated fit to three neutrino mixing: exploring the accelerator-reactor complementarity*, *JHEP* **01** (2017) 087, [[arXiv:1611.01514](#)].
- [60] A. Belyaev, N. D. Christensen, and A. Pukhov, *CalcHEP 3.4 for collider physics within and beyond the Standard Model*, *Comput. Phys. Commun.* **184** (2013) 1729–1769, [[arXiv:1207.6082](#)].
- [61] A. G. Akeroyd, M. Aoki, and H. Sugiyama, *Lepton Flavour Violating Decays $\tau \rightarrow anti-l \ell$ and $\mu \rightarrow e$ gamma in the Higgs Triplet Model*, *Phys. Rev. D* **79** (2009) 113010, [[arXiv:0904.3640](#)].

- [62] T. Fukuyama, H. Sugiyama, and K. Tsumura, *Constraints from muon $g-2$ and LFV processes in the Higgs Triplet Model*, *JHEP* **03** (2010) 044, [[arXiv:0909.4943](#)].
- [63] **ATLAS** Collaboration, M. Aaboud et al., *Search for doubly charged Higgs boson production in multi-lepton final states with the ATLAS detector using proton–proton collisions at $\sqrt{s} = 13$ TeV*, *Eur. Phys. J. C* **78** (2018), no. 3 199, [[arXiv:1710.09748](#)].
- [64] **ATLAS** Collaboration, G. Aad et al., *Search for anomalous production of prompt same-sign lepton pairs and pair-produced doubly charged Higgs bosons with $\sqrt{s} = 8$ TeV pp collisions using the ATLAS detector*, *JHEP* **03** (2015) 041, [[arXiv:1412.0237](#)].
- [65] A. Arhrib, R. Benbrik, M. Chabab, G. Moultaqa, M. C. Peyranere, L. Rahili, and J. Ramadan, *The Higgs Potential in the Type II Seesaw Model*, *Phys. Rev. D* **84** (2011) 095005, [[arXiv:1105.1925](#)].
- [66] R. N. Lerner and J. McDonald, *Gauge singlet scalar as inflaton and thermal relic dark matter*, *Phys. Rev. D* **80** (2009) 123507, [[arXiv:0909.0520](#)].
- [67] A. Schuessler and D. Zeppenfeld, *Unitarity constraints on mssm trilinear couplings*, *High Energy Physics - Phenomenology* (2007).
- [68] K. Kannike, *Vacuum Stability Conditions From Copositivity Criteria*, *Eur. Phys. J. C* **72** (2012) 2093, [[arXiv:1205.3781](#)].
- [69] K. P. Hadeler, *On copositive matrices*, *Linear Algebra & Its Applications* **49** (1983), no. FEB 79–89.
- [70] G. Chang and T. W. Sederberg, *Nonnegative quadratic bézier triangular patches*, *Computer Aided Geometric Design* **11** (1994), no. 1 113–116.
- [71] G. Bélanger, F. Boudjema, A. Goudelis, A. Pukhov, and B. Zaldivar, *micrOMEGAs5.0 : Freeze-in*, *Comput. Phys. Commun.* **231** (2018) 173–186, [[arXiv:1801.03509](#)].
- [72] A. Alloul, N. D. Christensen, C. Degrande, C. Duhr, and B. Fuks, *FeynRules 2.0 - A complete toolbox for tree-level phenomenology*, *Comput. Phys. Commun.* **185** (2014) 2250–2300, [[arXiv:1310.1921](#)].
- [73] Q. Yuan et al., *Interpretations of the DAMPE electron data*, [[arXiv:1711.10989](#)].
- [74] T. Bringmann and P. Salati, *The galactic antiproton spectrum at high energies: Background expectation vs. exotic contributions*, *Phys. Rev. D* **75** (2007) 083006, [[astro-ph/0612514](#)].
- [75] E. A. Baltz and J. Edsjo, *Positron propagation and fluxes from neutralino annihilation in the halo*, *Phys. Rev. D* **59** (1998) 023511, [[astro-ph/9808243](#)].
- [76] E. A. Baltz, J. Edsjo, K. Freese, and P. Gondolo, *The Cosmic ray positron excess and neutralino dark matter*, *Phys. Rev. D* **65** (2002) 063511, [[astro-ph/0109318](#)].
- [77] P. S. Bhupal Dev, D. K. Ghosh, N. Okada, and I. Saha, *125 GeV Higgs Boson and the Type-II Seesaw Model*, *JHEP* **03** (2013) 150, [[arXiv:1301.3453](#)]. [Erratum: *JHEP* 05, 049 (2013)].
- [78] P. A. Samuelson, *How deviant can you be?*, *Publications of the American Statistical Association* **63** (1968), no. 324 1522–1525.